Heart Rate Estimation Using Finger-Worn Accelerometers

University of Turku
Department of Computing
Master of Science (Tech) Thesis
Biomedical Engineering and Health Technology
February 2025
Omar Nasri

Supervisors:
Tero Koivisto
Jonas Sandelin

UNIVERSITY OF TURKU
Department of Computing

Omar Nasri: Heart Rate Estimation Using Finger-Worn Accelerometers

Master of Science (Tech) Thesis, 50 p.
Biomedical Engineering and Health Technology
February 2025

The purpose of this thesis is to examine the possibility of estimating heart rate with an integrated accelerometer using a finger-worn ring. In modern wearable devices heart rate monitoring is a highly common feature, with most using photoplethysmography (PPG) for this purpose. However, a clear challenge with PPG sensors is their relatively high power consumption, which is problematic for small devices with limited power supplies. This study presents a more power-efficient alternative method for heart rate estimation based on ballistocardiography (BCG). The objectives of this study are to determine whether heart rate estimation is possible from the finger using only accelerometers and whether this approach could be implemented into a commercial smart ring device to track sleep and heart rate.

To address these objectives, a custom-made ring was developed, containing an integrated accelerometer capable of recording 3-axis movement data. This ring was used to create a dataset containing BCG data from 23 subjects, with corresponding 3-lead ECG recordings used as the reference signal. Subsequently, an autocorrelation-based algorithm was developed to estimate heart rate from the BCG recordings using 10-second windows for analysis.

To study the possibility of integrating this solution into a commercial smart ring, more accurate estimations were attempted by filtering out signal windows with poor quality. This was accomplished by calculating several statistical metric values for each signal portion and setting threshold values that the metrics had to satisfy. Signal portions that failed to meet these criteria were excluded from heart rate estimation.

When comparing the heart rate estimations produced by the proposed algorithm to the reference ECG values without using signal quality-based filtration, an average mean absolute error of 1.88 bpm (beats per minute) was obtained. With the statistical signal quality filtration, this value improved to 1.40 bpm. Without the signal quality assessment, estimations were within ± 5 bpm 93.3 % of the time. When filtration was applied, this increased to 96.2 %.

The results demonstrate that this method has clear potential for implementation in commercial devices for heart rate estimation. This method performs especially well in scenarios with minimal motion artifacts, such as during sleep. Modern wearable devices already use accelerometers for sleep tracking, and implementing this method could eliminate the need for additional sensors.

Keywords: accelerometer, ballistocardiography, heart rate detection, sleep tracking, smart rings, wearables

TURUN YLIOPISTO
Tietotekniikan laitos

Omar Nasri: Heart Rate Estimation Using Finger-Worn Accelerometers

Diplomityö, 50 s.
Lääketieteellinen tekniikka ja terveysteknologia
Helmikuu 2025

Tämän tutkielman tarkoituksena on selvittää, voidaanko sykettä arvioida käyttäen ainoastaan älysormukseen integroitua kiihtyvyysanturia. Sykkeenseuranta on hyvin yleinen ominaisuus moderneissa puettavissa älylaitteissa, joissa sykkeen arviointiin käytetään yleensä fotopletysmografiaa (FPG). FPG:n merkittävin haaste on sen varsin korkea virrankulutus, joka on ongelmallista pienissä puettavissa älylaitteissa niiden rajallisen akkukapasiteetin vuoksi. Tässä tutkielmassa esitetään vaihtoehtoinen menetelmä sykkeen seurantaan, joka perustuu ballistokardiografiaan (BKG). Tavoitteena on määrittää, onko sykkeen mittaaminen mahdollista sormesta pelkän kiihtyvyysanturin avulla, ja selvittää voisiko tätä ratkaisua mahdollisesti hyödyntää kaupallisessa älysormuksessa sykkeen ja unen seurantaan.
Selvittääkseen vastaukset näihin tutkimuskysymyksiin kehitettiin erikoisvalmisteinen älysormus, joka sisältää integroidun kiihtyvyysanturin. Tätä sormusta käytettiin tietoaineiston laatimiseen, joka sisältää BKG-dataa 23 koehenkilöstä. Tietoaineisto pitää sisällään myös samanaikaisesti mitatun kolmekanavaisen EKG-tallenteen, jota käytettiin referenssisignaalina. Tämän jälkeen kehitettiin autokorrelaatiopohjainen algoritmi, joka arvioi sykettä BKG-tallenteista kymmenen sekunnin aikaikkunoissa. Selvitettäessä mahdollisuutta integroida tämäntyyppinen toiminnallisuus kaupalliseen älysormukseen, pyrittiin sykkeen seurannan tarkkuutta parantamaan suodattamalla pois huonolaatuiset signaali-ikkunat. Tämä toteutettiin laskemalla jokaiselle aikaikkunalle useita tilastollisia metriikka-arvoja ja määrittämällä raja-arvot, joiden tuli ylittyä. Signaaliosuudet, joissa nämä raja-arvot eivät ylittyneet, ei käytetty sykkeen arvioinnissa.
Kaikkien 23 signaalin keskiarvoisesta absoluuttisesta virheestä laskettu keskiarvo algoritmin sykearvion ja EKG-referenssiarvon välillä oli 1.88 lyöntiä minuutissa ilman signaalin laatuun perustuvaa suodatusta. Käytettäessä tätä suodatusta, arvo parani 1.40 lyöntiin minuuttissa. Ilman signaalin laatusuodatusta, sykearvioinnin virheet olivat ± 5 lyöntiä minuutissa 93.3 % ajasta, ja kun suodatus otettiin käyttöön, tämä kasvoi 96.2 %:iin.
Tuloksista ilmenee, että tällä menetelmällä on selkeästi potentiaalia hyödynnettäväksi kaupallisiin laitteisiin. Menetelmä toimii erityisen hyvin tilanteissa, joissa liikkeistä aiheutuvat häiriöt ovat minimaalisia, kuten nukkuessa. Nykyiset puettavat laitteet käyttävät jo kiihtyvyysantureita unen seurannassa, ja tämän menetelmän käyttöönotto voisi kokonaan poistaa tarpeen lisäantureille.

Asiasanat: ballistokardiografia, kiihtyvyysanturi, puettavat laitteet, sykkeen mittaus, unenseuranta, älysormukset

Contents

List of Figures

List of Tables

1 Introduction

Wearable devices have advanced notably, from their initial introduction in the 1960s [1]. Wearable technology is currently being incorporated into our everyday lives via devices like smartwatches, smart bracelets and smart rings. These devices can be used for everything from recording and analyzing vital signs like heart rate and blood oxygen saturation to even directly treating patients with devices such as smart insulin pumps [1]. One excellent example of a useful wearable device for healthcare is the Apple Watch, which is capable of recognizing atrial fibrillation using its built-in sensors and algorithms to monitor irregularities in heart rate and warn about cardiovascular abnormalities [2].

Wearable devices' clear potential together with recent advances in artificial intelligence, has caused an exponential increase in demand of these devices. Deloitte Global forecasted 320 million consumer health wearables to be shipped in 2022, with this expected to rise to 440 million units by 2024 [3].

Preventing morbidity and long-term disability in the hospital requires early detection of deterioration [4]. Vital signs monitoring, which seeks to detect physiological changes in deteriorating patients at an early stage, is thus widely used. Until recently, continuous vital signs monitoring was exclusively possible in hospitals' intensive care units (ICUs) [4], but with the popularization of wearable devices, it is now accessible to a wider public [5]. Reliable continuous monitoring of vital signs can be extremely helpful for diagnosing cardiac disorders including chronic obstruc-

tive pulmonary disease [6], myocardial infarction [7], atrial fibrillation [8], and many more.

The ease-of-use, aesthetic appearance, and power efficiency, enabled by the absence of a screen, have contributed to the rising popularity of smart rings [9]. As the industry standard method for heart rate monitoring, electrocardiogram (ECG) is often challenging to implement in these kind of wearable devices, photoplethysmogram (PPG) is commonly used instead [10]. A PPG sensor works by illuminating the tissues with a light-emitting diode (LED) and measuring the amount of light absorbed by the tissues, which generates a signal corresponding to heart cycles [11].

Ballistocardiography (BCG) offers an alternative method to PPG for approximating heart rate with a wearable device. BCG measures the body's recoil forces, caused by the blood's ejection into the vascular system [12]. Although the concept of BCG dates back to the 20th century [13], its practical applications have only recently seen significance, enabled by advancements in sensor technology and signal processing. Despite this progress, BCG remains a relatively novel technology with a strong focus in current research.

In this thesis, an alternative approach for the PPG is proposed based on the BCG signal measured using 3-axis accelerometer data. The accelerometer sensor is embedded into a custom-made smart ring, and the vibrations caused by the beating heart are used to detect heart rate. The primary advantage of this method is the considerably lower power consumption of the accelerometer sensor compared to the PPG sensor [14], which enables a much more power-efficient solution for continuous heart rate monitoring. The method is further supported by the widespread integration of accelerometer sensors in many popular wearable devices, which rely on accelerometer data for key features like activity tracking. This removes the need for additional hardware.

The heart rate values derived from the BCG data using the proposed method are

compared to reference values obtained from corresponding 3-lead ECG recordings using several performance metrics. Additionally, correlation analysis is performed to assess whether the results positively correlate with the reference values.

1.1 Research Questions

This study addresses these two research questions:

1. Can heart rate be accurately approximated from the accelerometer signal collected from the finger?

2. Can the proposed method be implemented in a commercial smart ring for tracking sleep and heart rate?

The first question is addressed by analyzing the data gathered with the custom smart ring and reviewing other related studies. Currently, no studies based on BCG signal acquisition from the finger exist. Therefore, in the literature review section of this thesis, research based on BCG signals recorded from the wrist is reviewed.

The second question is addressed by studying the affects of the signal quality metrics implementation on the results as in a commercial smart ring they could be used to potentially choose signals with minimal motion artifacts. Additionally, related studies are reviewed to understand how sleep tracking is currently performed on commercial wearable devices and to identify further methods for reducing motion artifacts using the accelerometer data itself.

1.2 Thesis content summary

The later sections in this thesis are structured as follows: Chapter 2 introduces the background concepts needed for this thesis including modern health care wearables, PPG, ECG, accelerometers with BCG, and digital filters. Chapter 3 presents ear-

lier studies related to sleep tracking with wearable devices, other BCG heart rate estimation techniques, use of autocorrelation in heart rate detection, advantages of accelerometer sensor over PPG and the motion artifact reduction techniques using accelerometer data. The custom smart ring device used for data recording and the formulated dataset are described in Chapter 4. Chapter 5, explaines the proposed method in detail and the results obtained with this method are presented in Chapter 6. The results are discussed in Chapter 7 and finally, the thesis is concluded in Chapter 8.

2 Background

2.1 Wearables

In health care, wearables refer to devices worn by patients to assist in monitoring and diagnosis. These devices are often inexpensive and provide an easy method for continuous monitoring, with the advantage of minimizing discomfort and avoiding interference with daily activities. By wearing these devices, individuals can actively engage in managing their own health, gaining insights and tracking important metrics over time. The potential of wearable devices is vast and for example the NHS (National health service) in UK has placed medical wearable devices on their strategic long-term plan. It is anticipated that wearables will become increasingly advanced and make significant contributions to the health care sector. [15]

Many wearable sensors have already been accepted by the U.S. FDA (United States Food and Drug Administration) for use as medical devices and are being adopted into standard clinical practices. These wearable sensors can be classified into three primary categories: mechanical, physiological, and biochemical. The data collected from these different sensor types are used for a variety of applications, including atrial fibrillation detection, heart rate monitoring, and walking analysis. Some examples of devices that have met the FDA standards of wearable devices can be seen in Table 2.1. [16]

Wearable mechanical sensors often incorporate inertial measurement units (IMUs),

which consist of accelerometers, gyroscopes and magnetometers to estimate and track subjects' 3D movement and orientation [16].

Physiological sensors detect biosignals using various methods such as optical, electrical, acoustic, or thermal sensing. These signals include vital signs like heart rate, blood pressure, and blood oxygen levels, along with bodily functions such as respiratory rate and bioelectrical activities like ECG and EEG. [16]

Biochemical sensors, on the other hand, convert chemical or biological analyte into an electrical signal and they are often related to clinical applications. Biochemical signals have a wide range of uses including glucose monitoring, alcohol detection and pH testing. [16]

Brand	Model	Type	Sensors	Reference
Apple	Watch	Smartwatch	ECG, PPG, ACC, Gyro, GPS	[16], [17]
Dexcom	Stelo	Continuous Glucose Monitor patch	Glucose biosensor (CGM)	[18], [19]
Zoll	Lifevest	Wearable defibrillator	ECG	[16]
Ava Science, Inc.	Ava Wristband	Menstruation and fertility tracking	ACC, EDA, PPG, temperature sensors	[16], [20]
iRhythm	Zio Patch	Long term heart monitor patch	ECG	[21]

Table 2.1: Examples of FDA-approved wearable devices. Abbreviations used in the table: Electrocardiogram (ECG), Photoplethysmogram (PPG), Accelerometer (ACC), Gyroscope (Gyro), Global Positioning System (GPS), Continuous Glucose monitor (CGM) and Electrodermal activity (EDA).

2.2 Photoplethysmogram

Photoplethysmography (PPG) is an optical technique used to obtain signal corresponding to changes in blood volume within tissue. It is a non-invasive method that measures how much light is absorbed or reflected by the human tissue. The

resulting signal contains valuable information about the cardiovascular, respiratory and nervous systems. Clinically, PPG is the most commonly used method for measuring blood oxygen saturation and heart rate, offering a simple and non-invasive method of monitoring these key vital signs. Recently, interest in PPG has increased significantly due to the growing demand for affordable and simple technologies in the health technology industry, driven by the increasing focus on wearable devices. [11]

A standard PPG device typically consists of a light source, often a LED (Light-emitting diode) and a photodetector. When the light source emits light to the tissue, the amount of reflected light is measured by the photodetector. The resulting signal, which represents the variation in reflected light, corresponds to the blood pulsations induced by the heartbeat. Most common LED colors used in clinical trials are red, green and infrared, as light with longer wavelengths penetrates the tissue more effectively [22]. The green LED is generally used for heart rate estimation [23] and the red and infrared for blood oxygen saturation calculation [24]. The resulting PPG signal can be characterized by two main features: the systolic and diastolic points, which can be seen in Figure 2.1. The diastolic point marks diastole, where blood pressure is at its minimum, while the systolic point marks the beginning of systole, when the heart starts pumping blood and blood pressure reaches its maximum [25]. Diastole period is the period between these two points, where the blood begins filling the heart. The dicrotic notch is also visible from the PPG; it has been considered as an indicator of arterial stiffness, which can be an important marker in cardiovascular health of an individual [26].

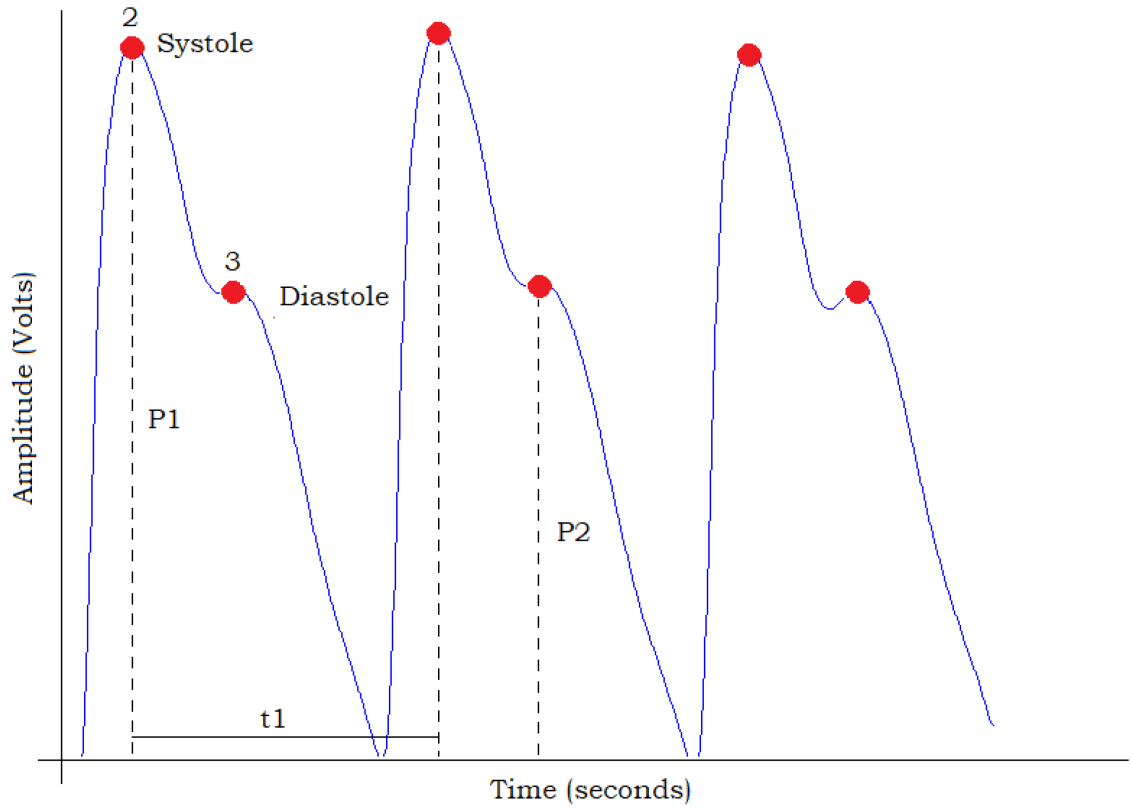

Figure 2.1: Typical PPG signal [25]

2.3 Electrocardiogram (ECG)

Electrocardiogram is a recording of the heart's electrical activity and represents its cardiac cycles, providing a time-voltage chart of the heartbeat [27]. ECG is crucial when evaluating patients with potential cardiac-related issues. The goal is to determine whether ECG recordings are normal or pathological [28]. In cardiac cycle the activation of heart cells is termed depolarization and contrarily, the heart cells return to resting state is referred to as repolarization. The resting heart muscle cells are polarized, meaning they carry an electrical charge on their surface. When the cell is stimulated, it begins to depolarize and a small electrical current is formed, which propagates along the length of the cell. Repolarization occurs after the fully depolarized cell returns into its resting state, and spreads until the whole cell is again

repolarized. ECG consists of these two events, making them essential for assessing whether the ECG is normal or abnormal. [29]

In an ECG recording, there are five basic waveforms that represent the functionality of the heart: P-wave, QRS complex, ST-segment, T-wave and U-wave. The SA node is responsible for regulating the heart's pacing. It is a cluster of muscle cells in the heart that can spontaneously generate an electrical impulse, which is then spread throughout the heart [30]. The depolarization initiated by the SA node, is represented by the P-wave, with the first half corresponding to right atrial depolarization and the second half to left atrial depolarization. The QRS complex reflects ventricular depolarization and contraction. The ST-segment represents the end of ventricular depolarization, and the beginning of the repolarization of the ventricles. Consequently, the following T-wave naturally represents the ventricular repolarization phase. Similarly, the U-wave is also related to the ventricular repolarization; it is a small wave that follows the T-wave. It represents the delayed repolarization of Purkinje fibers, which are specialized cardiac muscle fibers in the impulse-conducting network, that quickly transmit electrical impulses to the ventricles [31]. The atrial repolarization is generally not visible from the ECG due to the low amplitudes of the atrial ST-segment and T-wave.[28], [29]

The body conducts the electrical currents produced by the heart, which can be measured using a recording instrument. In a clinical setting, the most common method for recording these currents is with the 12-lead ECG. These leads capture the differences in voltage between electrodes and display them; the use of multiple leads is necessary to provide a broad view of the heart's electrical activity. The electrode placements in a 12-lead ECG, along with an example ECG signal, are shown in Figure 2.3. [32]

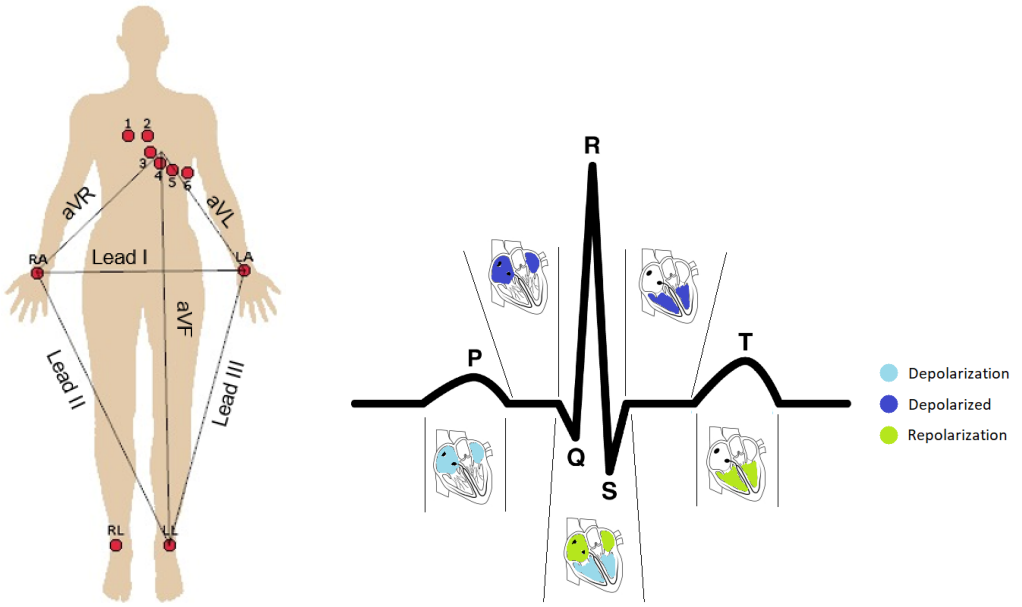

(a) Electrode placement in the standard 12-lead system [33].

(b) ECG heart cycle representing the basic waveforms along with the associated depolarization and repolarization events [33].

Figure 2.2: Electrode placement and ECG waveform.

2.4 Accelerometer

An accelerometer is a sensor that measures acceleration, which describes the amount of change in velocity over time [34]. It is often used in many different applications to detect motion, orientation, and vibration. They can be used in several body locations, with the most common ones being the wrist or thigh [34]. Modern accelerometers generally measure acceleration in 3 axes, with the acceleration data representing the direction and magnitude of acceleration in each axis [34]. The unit of acceleration in the raw data is g, where 1 g equates to the gravity on earth. Advances in accelerometer design have significantly reduced the cost and power consumption of these sensors, enabling their use in wearable devices such as smartwatches, bracelets and other various use cases. [35].

The properties of the data captured by accelerometers can vary, depending on

the sampling rate and the captured acceleration range. In this context, the sampling rate refers to the frequency of which the recording is captured; it is stated by the Nyquist theorem that, in order to sufficiently capture a signal, the sampling rate needs to be at least double the frequency and most sensors used for physical activity measurement use the sampling range of 30-100 Hz. In motion detection with accelerometers, the acceleration intensities can be as high as 6 g, but for heart rate estimation, low measurement ranges are sufficient, as the captured movements are fairly subtle. [34]

A common challenge associated with accelerometer recordings is their sensitivity to noise and outliers. Since accelerometers capture even the subtlest movements, a significant amount of noise can be introduced into the recordings [34]. While various digital filter designs can often mitigate this noise, finding the right balance between retaining the important features of the signal and filtering out irrelevant noise can be quite challenging.

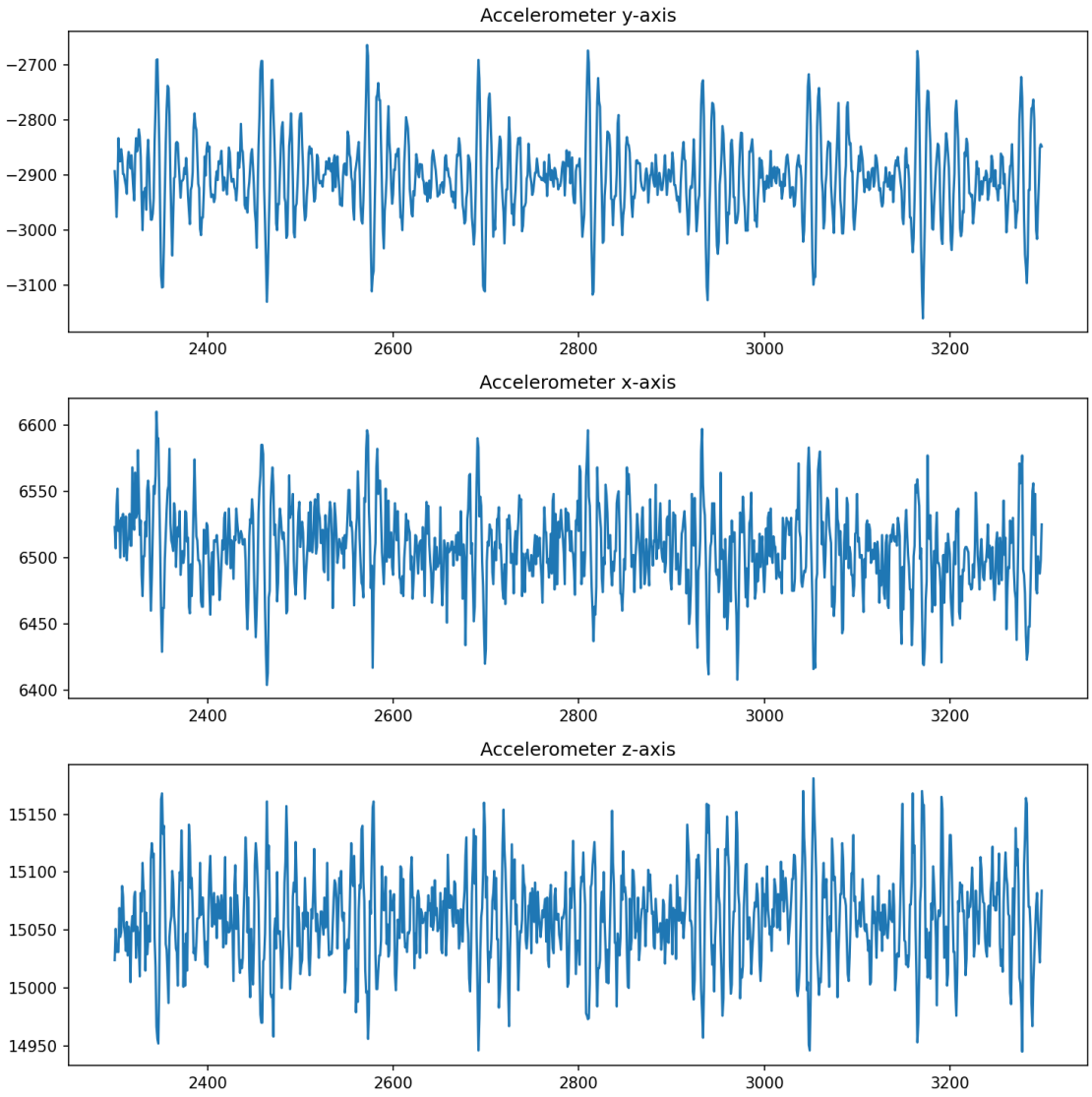

Figure 2.3: Raw 3-axis accelerometer signal: Heart cycles are visible on all three axes, but the Y-axis contains the least noise.

2.4.1 Ballistocardiography (BCG)

Ballistocardiogram measures the body's recoil forces in response to cardiac blood ejection into the vascular system. This non-invasive method tracks body motion generated by each cardiac cycle's blood ejection [12], [36]. At every heartbeat the travelling blood causes subtle changes in the body's center of mass. These changes

generate micromovements, driven by recoil forces that help maintain the body's momentum [12]. The magnitude and direction of these recoil forces fluctuate in response to the cardiac cycle and the BCG is a recording of these movements [37]. The BCG signal can be measured as displacement, velocity, or acceleration, capturing motion across all three axes [12].

There are several methods for BCG signal acquisition. Modern wearable BCG systems rely mostly on accelerometer-based approaches. In these solutions, the sensor is attached to the body, typically on the chest or wrist. As long as the sensor is securely affixed to the body, the recoil forces are expected to be detectable by the externally attached accelerometer. These systems provide a simple method of continuously monitoring the heart; however, they are highly sensitive to motion artifacts. As noted in 2.4, motion artifacts often constitute a significant challenge when using accelerometers a less motion-sensitive approach to recording BCG signal is to use a bed-based BCG system. These are typically used to monitor sleep, or vital signs of bedridden patients. In these applications, different sensors such as strain gauges, load cells or vibration sensors are typically placed under the bed, mattress or sheet, to record the BCG signal. Although these systems are less sensitive to motion artifacts, several challenges remain with BCG recordings as interpersonal variability, influenced by factors such as age, body position, and gender, affect the quality of the recordings [38]. Even the bed itself, or the thickness of the mattress can have an impact on the recordings [39]. [40]

Cardiovascular diseases are a leading cause of death in modern society and many of these conditions are preventable and treatable with appropriate screening. Analysis of the BCG signal can provide valuable insights into heart health; a healthy heart typically generates large waveforms with strong contractility, while a weakened heart produces only small waveforms. It has been shown that BCG has the ability to detect cardiac changes in the early stages, making it a promising tool for

early intervention. Factors such as age and physical activity levels can also have an effect on the BCG signal amplitude, with older people exhibiting significantly decreased signal amplitudes even in the absence of underlying cardiovascular abnormalities. Given its capability for continuous monitoring, ballistocardiography serves as an effective diagnostic tool for identifying conditions like atrial fibrillation, heart failure, and other cardiac abnormalities [41]. [42]

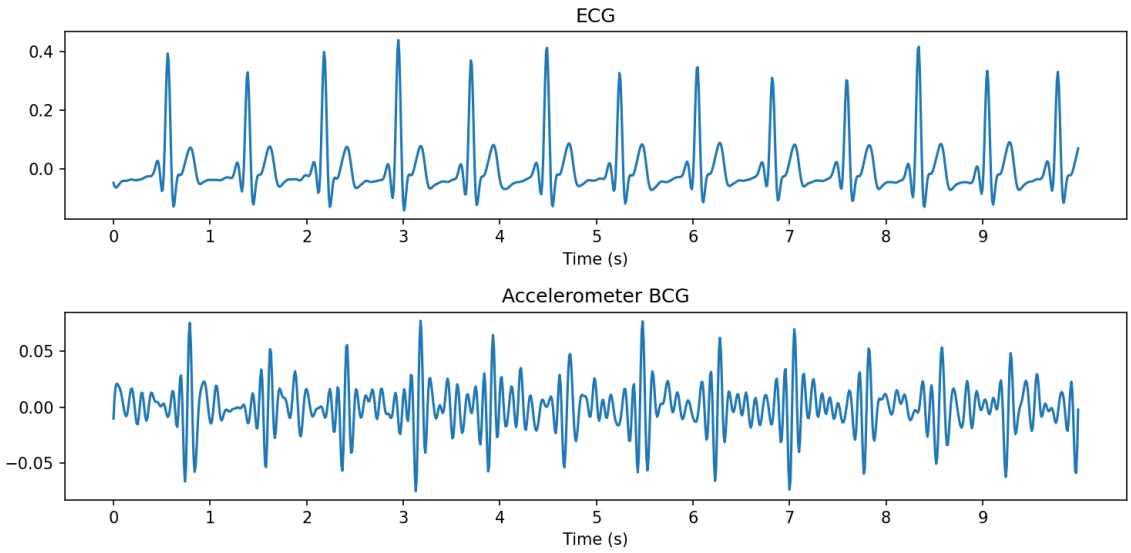

Figure 2.4: Bandpass filtered Ballistocardiography (BCG) signal recorded from the finger, displayed alongside the corresponding bandpass filtered electrocardiogram (ECG) recording above.

2.5 Digital filters

As stated in 2.4.1, BCG signals, particularly those recorded using accelerometers, are often mixed with motion artifacts and other noise. Therefore, it is necessary to employ techniques that minimize these interferences and selectively extract heart cycles from the signal. In BCG analysis, digital filters are often used to achieve this. Digital filters are tools to separate mixed signals, such as fetal ECG signals from maternal ECG signals during pregnancy, or to isolate specific components from

signals that have been combined, as is often the case with BCG. These filters most commonly work by manipulating the sampled data either by convolution or recursion [43]. In this chapter, the digital filters used in this study are introduced.

2.5.1 Butterworth Band-pass filter

Butterworth filters are digital filters designed to have mathematically flattest possible frequency response within a specified passband. They allow signals within this band to pass through without significantly modifying the signal strength. The filter's order determines the steepness of the cutoff between the passband and the stopband, with higher orders yielding more accurate output results. Due to their frequency-based nature, the filtering effects are easily understood and predicted. This simplicity, combined with high performance levels, accounts for their widespread usage. [44], [45]

Butterworth band-pass filter, which allows a specific frequency range to pass, is created by combining Butterworth low-pass and high-pass filters [44]. Low-pass filters allow lower frequencies to pass while blocking higher frequencies that exceed the cutoff frequency. In contrast, high-pass filters allow frequencies above the cut-off frequency to pass, and those below are attenuated [45]. In ballistocardiography (BCG), heart cycles typically fall within the frequency range of 1-12 Hz [41]. Consequently, the frequency range used in the filtration stage of this thesis is 0.5-15 Hz. The affect of band-pass filteration on a BCG signal can be seen in Figure 2.5.

2.5.2 Moving average filter

The most common filter designs focused on the process of noise reduction or smoothing are based on averaging. The moving average filter is particularly well suited for reducing random noise in accelerometer data. Due to the sharp step response of the filter, significant distortions can be produced by moving average filter [46]. Con-

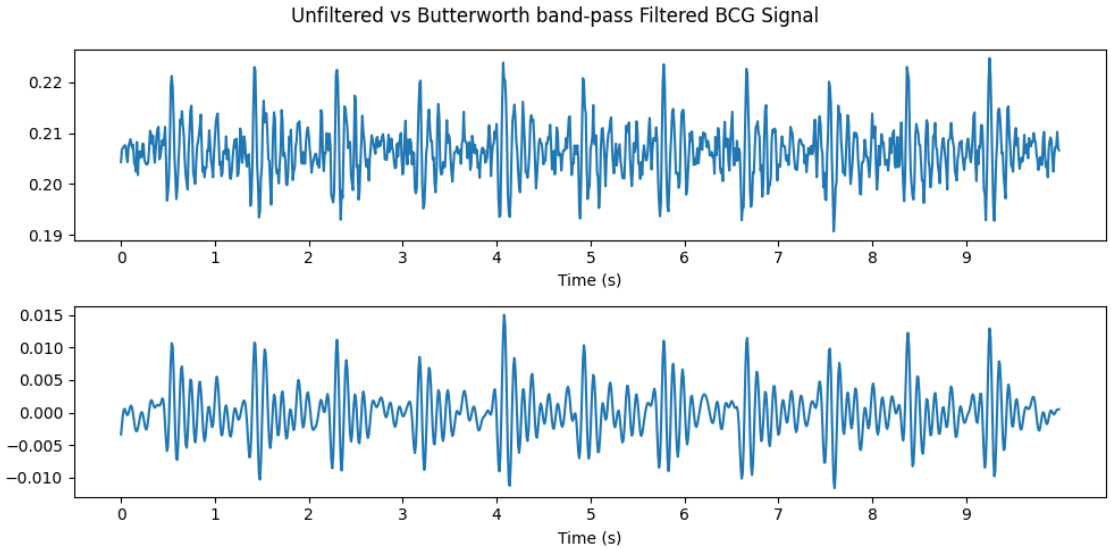

Figure 2.5: Raw ballistocardiography (BCG) signal recorded with the smart ring device is shown above, with the Butterworth band-pass filtered version below.

sequently, in this study, this filter is applied to the autocorrelation function of the ballistocardiography signal, which can be seen in Figure 2.6.

Moving average filter averages a certain number of points from the input signal to generate the output signal. This process is repeated over a moving window, where a predetermined number of points is utilized to calculate the average of the dataset [46]. The resulting output is a smoothed version of the signal, and the amount of smoothness is dependent on the selected window size.

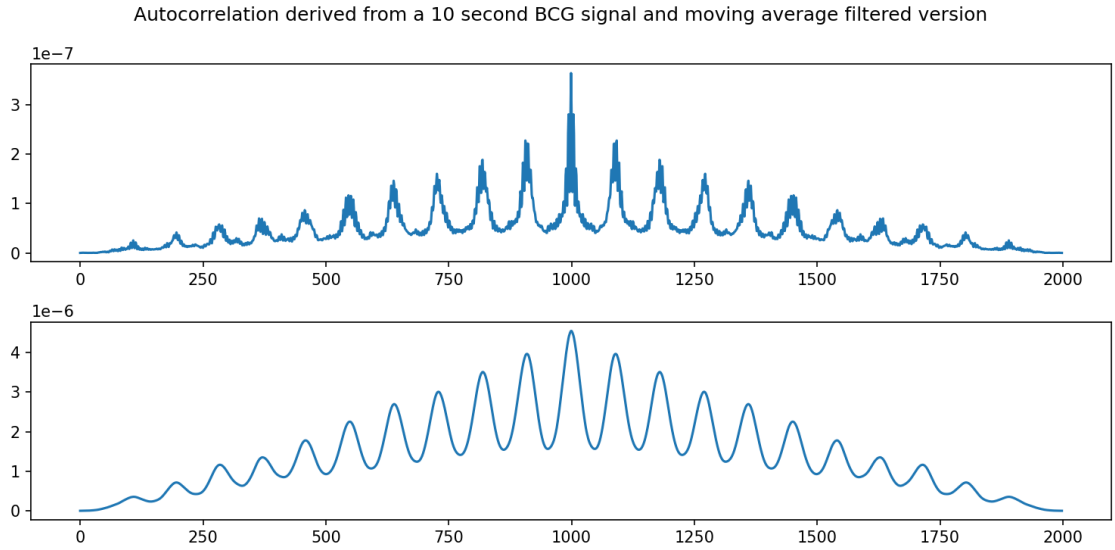

Figure 2.6: Autocorrelation function obtained from a 10 second segment of BCG signal. The signal was squared to emphasize the peaks in the BCG data corresponding to heart cycles. The bottom signal represents the moving average filtered version of this autocorrelation result.

3 Related work

3.1 Sleep tracking with wearable devices

Sleep disorders are a common health issue in individuals and almost every other person has experienced some form of sleep related disorders. These disorders pose a significant risk to both physical and mental health, as mental health problems are often associated with various sleeping disorders [47].

Normal sleep consists of a certain number of sleep cycles. An individual who sleeps for 8 hours typically goes through around 5 sleep cycles each night, with each complete cycle lasting about 90 to 110 minutes [48]. Sleeping can be separated into two main types: REM (rapid eye movement) and non-REM sleep. A normal sleep cycle includes the following stages: wakefulness, light sleep (Stage 1), deeper sleep (Stage 2), deepest non-REM sleep (Stage 3), and REM sleep [48], with stages 1-3 considered being non-REM stages.

During the light sleep stage, the brain activity begins to slow down, while skeletal muscle tone, breathing rhythm and heart rate remain regular. In the deeper sleep phase, heart rate and body temperature decrease, and in the deepest non-REM sleep, there is minimal brain activity as the body restores its tissues. REM sleep is the final stage in the sleep cycle, and it is often associated with dreaming. In REM sleep the heart rate is significantly higher and more irregular than in the light sleep stage [49]. Although the electrical activity of the brain resembles that of an awake

person, breathing also becomes irregular and skeletal muscles are atonic, except for the eyes and diaphragm. [48]

The gold standard for sleep monitoring is the polysomnography, which uses sensor fusion to assess and monitor individuals sleep [47]. The sensors used in polysomnography often measure electrical activity of the brain, electrical activity in the muscles, airflow through the respiratory system, heart rate, pulse oximetry and thoracic movements. These measurements have to be completed in a controlled laboratory setting. The limitation of this method is that the subjects must attempt to sleep normally in an unnatural environment, with several sensors attached to them.

This limitation can be addressed by using wearable devices. The most commonly used sensor for sleep tracking is the accelerometer, as it is able to track muscle tone and breathing rhythm [14]. Many devices also use the heart rate sensor to measure heart rate variability, which can be used to identify the stages of sleep [47]. Modern commercial wearable devices used for sleep monitoring are typically smartwatches or smart bracelets.

3.2 Accelerometer-based heart rate monitoring through Ballistocardiography

Currently, there are no studies specifically focused on BCG signal recordings from the finger for heart rate approximation. Therefore, this chapter will focus on BCG measurements from the wrist, which are more thoroughly researched than finger-based methods, particularly using wearable devices such as smartwatches or activity bracelets. The wrist serves as a relevant point of reference for discussing BCG-based heart rate estimation, due to its popularity in current technology and similarity with finger measurements [50], [51].

Promising results were obtained in [14], with a similar study setup to the one presented in chapter 5 of this thesis. Accelerometer mounted to the wrist, was used to detect several vital signs (HR, respiration rate, muscular microvibrations) while being at a resting position. The HR value obtained with the accelerometer was compared to a reference heart rate, which in this case, was the HR acquired with a pulse oximeter. Additionally, the accelerometer values were also compared to measurements from an LG smartwatch and a blood pressure monitor. The algorithm proposed in this study, worked in three filtering stages, which was used to estimate these key vital signs. As is often the trait with accelerometer data, the measured motion is split into 3 axes. To preserve information from all three axes, instead of discarding two, the vectors are combined by calculating the total acceleration as the vector magnitude: $|\vec{a}| = \sqrt{a_x^2 + a_y^2 + a_z^2}$. Subsequently, the combined acceleration data was low-pass filtered to extract the low-frequency breathing rhythm and high-pass filtered to capture the high-frequency microvibrations of the body. Lastly, the data was processed using a squaring algorithm to highlight the heart cycles. In the study, it was determined using a Tukey HSD statistical test [52] that the heart rate estimations from the accelerometer and the blood pressure monitor did not show any significant differences compared to the pulse oximeter values. Therefore, it was concluded that both devices were capable of successfully detecting the heart rate. However, surprisingly, the LG smartwatch performed significantly worse, with a mean error of 5.58 %. Table 3.1 displays the heart rate results obtained from the different devices.

Similar research work is presented in [53], with a higher focus on the removal of motion artifacts and noise, from the accelerometer signal; in this study, it was noted that the primary limitation in continuous heart rate approximation using accelerometers is the significant amount of random motion artifacts introduced into the data. Various signal decomposition algorithms performances were compared in the pro-

Table 3.1: Heart rate measurement results from [14] with various devices, including the corresponding error percentages for each participant.

Participant	**Reference Pulox (bpm)**	**Accelerometer (bpm, % Error)**	**BP Monitor (bpm, % Error)**	**LG Watch (bpm, % Error)**
P01	70	69 (1.43%)	69 (1.43%)	73 (4.29%)
P02	67	67 (0.00%)	66 (1.49%)	66 (1.49%)
P03	66	67 (1.52%)	65 (1.52%)	69 (4.55%)
P04	68	69 (1.47%)	70 (2.94%)	67 (1.47%)
P05	64	62 (3.13%)	62 (3.13%)	62 (3.13%)
P06	71	70 (1.41%)	70 (1.41%)	77 (8.45%)
P07	67	67 (0.00%)	72 (7.46%)	73 (8.96%)
P08	68	67 (1.47%)	69 (1.47%)	66 (2.94%)
P09	73	72 (1.37%)	72 (1.37%)	79 (8.22%)
P10	63	60 (4.76%)	61 (3.17%)	59 (6.35%)
P11	70	70 (0.00%)	72 (2.86%)	68 (2.86%)
P12	81	82 (1.23%)	80 (1.23%)	78 (3.70%)
P13	82	78 (4.88%)	79 (3.66%)	78 (4.88%)
P14	58	57 (1.72%)	57 (1.72%)	70 (20.69%)
P15	56	56 (0.00%)	56 (0.00%)	57 (1.79%)
Mean Dev.		1.63%	2.32%	5.58%

cess of removing this noise, with a primary focus in variable mode decomposition (VMD) and singular spectrum analysis (SSA). Typically, the SSA decomposition algorithm requires multiple data sources; however, since the accelerometer signal is three-dimensional, SSA was applied using this 3D data. The resulting decompositions from these methods were assessed to identify the frequency components, where the heart rate signal was present. Kalman smoothing was found to have the best results in continuous HR tracking, so it was used to filter out the noise and smooth the data. A wrist-worn device was then designed, containing an integrated accelerometer. The algorithms were then tested on 20 subjects during different tasks, such as finger tapping, typing, and various hand movements. Several performance metrics were used to estimate the accuracy of the methods against the reference HR, which in this study was measured using ECG chest strap heart rate monitor. These metrics are displayed below.

- The average absolute deviation:

$$\epsilon_1 = \frac{1}{N} \sum |HR_{\text{Acc}} - HR_{\text{ECG}}|$$

- The maximum absolute deviation:

$$\epsilon_2 = \max |HR_{\text{Acc}} - HR_{\text{ECG}}|$$

- The standard deviation:

$$\epsilon_3 = \sqrt{\frac{1}{N} \sum |HR_{\text{Acc}} - HR_{\text{ECG}}|^2}$$

Results obtained from the subjects are illustrated in Table 3.2. These findings indicate that the SSA, combined with Kalman smoothing, meets the accuracy standards for medical devices established by the American National Standards Institute (ANSI) more than 90 % of the time. According to these standards, the heart rate must fall within 10 % or within 5 beats per minute (bpm), whichever is greater. [53]

3.2.1 Autocorrelation in heart rate detection

Autocorrelation is a statistical measure, that describes the relationship of a signal and it's lagged versions of itself. It is a representation of how much the signal correlates with itself, at different points of time. For successive and completely uncorrelated observations, the autocorrelation function is zero. However, for example periodical, or quasi-periodical signals, such as heart rate, the autocorrelation function reflects these repeating patterns [54]. This can be seen in Figure 2.6, where the autocorrelation derived from the BCG signal clearly displays the heart cycles.

Several heart rate estimation techniques utilize autocorrelation due to the distinctive signal morphology produced by the heartbeat. Numerous algorithms have

Table 3.2: Values of ϵ_1, ϵ_2, and ϵ_3 for VMD and SSA in [53].

	VMD			**SSA**		
No.	$\boldsymbol{\epsilon_1}$	$\boldsymbol{\epsilon_2}$	$\boldsymbol{\epsilon_3}$	$\boldsymbol{\epsilon_1}$	$\boldsymbol{\epsilon_2}$	$\boldsymbol{\epsilon_3}$
1	2.11	6.25	2.51	1.72	6.54	2.06
2	4.09	13.56	4.38	2.01	6.21	2.35
3	2.77	9.3	3.07	2.38	9.92	2.98
4	4.12	14.91	3.59	3.84	9.18	4.57
5	2.96	10.81	3.27	3.53	8.76	4.25
6	3.88	9.68	3.58	2.66	7.6	2.98
7	7.75	20.27	6.82	7.38	18.69	6.92
8	7.35	19.97	7	3.77	12.42	4.22
9	2.63	9.68	3.29	2.47	7.29	3
10	2.53	6.92	3.01	3.76	9.18	2.61
11	8.28	34.04	11.96	4.78	10.52	5.58
12	3.96	11.81	4.56	4.4	15.77	5.28
13	7.77	16.43	5.22	3.62	8.61	2.7
14	5.05	17.09	5.91	5.12	13.23	5.86
15	5.41	19.89	6.61	4.33	15.58	5.32
16	8.34	12.9	2.37	2.42	7.23	2.83
17	5.06	13.83	5.65	4.49	9.17	4.67
18	8.13	18.1	8.53	5.5	11.82	5.87
19	4.01	10.95	4.99	2.6	6.83	3.1
20	7.23	24.81	7.29	3.14	8.33	2.64
Avg	5.17	15.06	5.18	3.70	10.14	3.99

succesfully applied different autocorrelation algorithms, to estimate heart rate and some are presented in [38], [55], [56]. These papers present different methods to detect signal periodicity, with the highest peaks in the output typically corresponding to heartbeats.

The most common challenge in using autocorrelation for heart rate detection is the natural variability between heartbeats, which is perfectly normal for a healthy heart. This can reduce the accuracy of algorithms based on autocorrelation, as the heart's signal is not perfectly periodical [56]. Naturally, other irregularities, such as arrhythmias, can also have a significant impact on the resulting autocorrelation function. For this reason, autocorrelation is often applied to short signal segments or windows, such as 5 seconds, which helps minimize the impact of heartbeat variability

over time.

3.3 Advantages of Accelerometer sensor over PPG

The purpose of this thesis is to determine whether the accelerometer alone is capable of accurate heart rate monitoring in wearable devices. The accelerometer has several advantages over PPG, which is well established industry standard for heart rate detection in wearables [10]. These advantages include significantly lower power consumption, simultaneous movement and physical activity detection, and the fact that accelerometers are found in a wider range of devices [14].

Long term continuous monitoring of biosignals is a key element in mobile health care. Wearable devices enable easy and unintrusive monitoring of important vital signs, which is one of the most important features of these devices. However, the relatively high power consumption of the PPG sensor is the reason why the sensor is ineffective for long-term or continuous monitoring of the heart rate [57]. Despite the relatively high efficiency of LEDs, commercial PPGs still require about 20-60 mW of power during continuous operation [58].

The power consumption value of the accelerometer sensor is influenced by several factors, including sampling rate [59], measurement range [60] and power supply voltage [61]. Heart rate tracking does not require very demanding sensor settings from the accelerometer. The sampling rate of the recording must be at least twice the maximum frequency component of the signal as outlined by the Nyquist theorem [62] and as stated in 2.4 the heart cycles in BCG fall within the range of 1-12 Hz. This means that in theory a sampling rate of 24 Hz should be sufficient. Additionally, the small micro-movements produced by the beating heart can be detected with a relatively low sensor range. Some sensors reported in, [63], [64] have power consumptions of 2.2 mW, 4.5 mW, respectively. Comparing these values to the PPG sensors, we can conclude that in continuous operation accelerometers gener-

ally consume considerably less power. This is also supported by a study [14] where the consumption of the PPG is estimated to be in the range of 1-50 mW, while accelerometer is approximated to fall within the range of 0.5-2 mW.

3.4 Reducing motion artifacts in heart rate estimation using accelerometers

Heart rate estimation is significantly affected by motion artifacts of the body, as discussed in earlier chapters. This thesis introduces an accelerometer-based approach for heart rate approximation, that relies on a high-quality BCG signal, which requires the body to remain relatively stationary during the measurement process. The implemented algorithm is not designed for recordings with significant noise, such as during physical activity, but rather for scenarios where the body remains fairly stationary, such as during sleep. To address this, various techniques employing accelerometer data to remove and recognize motion artifacts were explored.

Adaptive filters are digital filters that utilize adaptive coefficients. In these filters, an adaptive algorithm updates the filter's coefficients based on a specific reference signal [65]. The desired part of a signal can be extracted from the noisy part by using a signal that represents the noise as a reference signal. Promising results have been achieved in PPG noise reduction by using the accelerometer data as the reference signal [66]. In this solution, the accelerometer data is used to represent the noise, and the filter's coefficients are adjusted accordingly to reduce noise in the output signal. In [67] an ear-based PPG system is introduced where an adaptive filter is employed using the vertical accelerometer axis as a noise reference input. The system is tested in three physical activities: standing, walking, and running, and then compared to the ECG reference value. Linear regression indicated a high correlation between the heart rate estimations of the proposed device and ECG in

all three conditions: standing = 0.97, walking = 0.82 and running = 0.76.

A motion artifact reduction technique based on accelerometer spectrum analysis is presented in [68]. In this algorithm, the accelerometer's frequency content is computed, and the resulting spectrum is used to identify the motion artifact frequencies. Band-stop filter is then applied to the original signal to remove this noise and the resulting signal is then used to estimate the heart rate. This solution was tested by placing the reference PPG sensor on the subject's stationary right hand, while having the other sensor on the subject's left hand, which was allowed to move. Using this method, a mean absolute error of 0.8 bpm compared to the reference HR was obtained for the motion artifact-reduced signal, compared to 2.1 bpm for the original heart rate estimation against the reference.

A simpler approach is to use purely statistical calculations to detect motion artifacts. Metrics such as skewness, which measures asymmetry, and kurtosis, which describes the peakedness of the distribution, are popular choices in these solutions. These metrics are useful for identifying corrupted and artifact-free signals, as they tend to display higher magnitudes in motion-corrupted data [69]. By setting threshold values for these metrics, the noisy and motion-corrupted signal components can be removed or marked as potentially inaccurate [66].

Selecting the appropriate threshold values can be challenging as there are no universal guidelines on how to set them optimally for different conditions. Moreover, these thresholds can potentially require adjustment for individual differences, as BCG morphology is affected by each person's unique physiological qualities, as described in Chapter 2.4.1.

4 Dataset description and measurement process

A custom-made measurement device was used for data collection (Figure 4.1). The device consists of an inertial measurement unit (Bosch Sensortec BMI160) and an 3-lead ECG sensor (Texas Instruments AD8232). The analog ECG signal is read with Texas Instruments ADS1015 ADC. The IMU is mounted to a plastic housing, which is attached to an adjustable ring. The device was set to record accelerometer data with a measurement range of ±2g. Both IMU and ECG data were recorded with a sampling rate of 100 Hz, and the signals were synchronized by recording the timestamps from the microcontroller unit during sampling and aligning these timestamps.

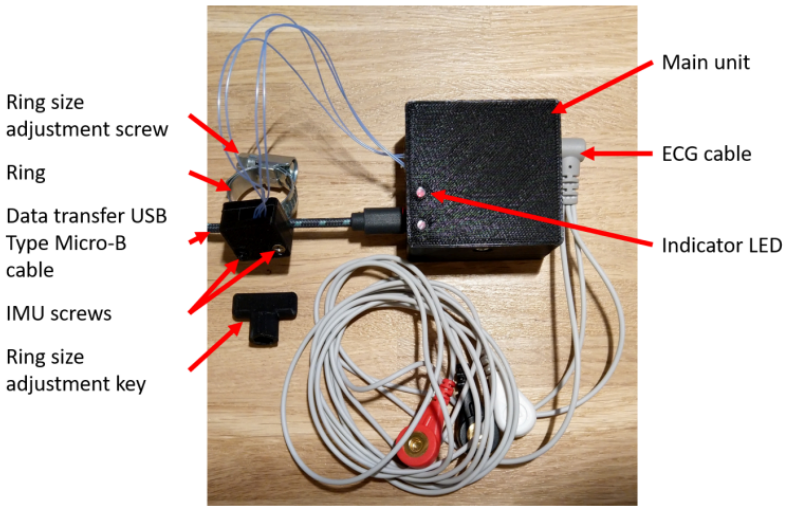

Figure 4.1: The smart ring device used for data acquisition.

The dataset was collected with the described device at University Of Turku from 23 participants employed in the Department of Computing, all of whom were in good overall health. The formulated dataset is described in Table 4.1. The gyroscope measurements were not used in this thesis.

The subjects were laying on a bed with their hands on their sides. The device was then attached by placing 3 electrodes (left arm, right arm, left leg) onto the study participants. Consequently the ring was adjusted to fit the subjects left index finger, ensuring that the ring was pointing upward so that the accelerometer axes were properly leveled. Once the signals from both sources were found to be satisfactory, the recording was started. Five minute recordings were obtained.

Variable	**Description**
imu_timestamp	Timestamp of the IMU data
acc_x	Acceleration in the X-axis
acc_y	Acceleration in the Y-axis
acc_z	Acceleration in the Z-axis
gyro_x	Angular velocity in the X-axis
gyro_y	Angular velocity in the Y-axis
gyro_z	Angular velocity in the Z-axis
ecg_timestamp	Timestamp of the ECG data
ecg	ECG value

Table 4.1: Descriptions of the Dataset Variables

5 Proposed method description

The raw accelerometer data obtained with the smart ring device requires several signal processing steps to achieve the optimal results. In a study by Haescher et al. [14] a very similar study setup is presented, and the introduced signal processing steps are used as a general guideline in this thesis. After the necessary pre-processing steps are completed on the accelerometer data, the recordings are divided into shorter windows, and autocorrelation is calculated to capture the periodical heart cycles. Peak detection algorithm is then applied to detect the peaks corresponding to each heartbeat within the autocorrelation signal. By measuring the time interval between these peaks, the heart rate is estimated. This process (Figure 5.1) is explained in detail in this chapter.

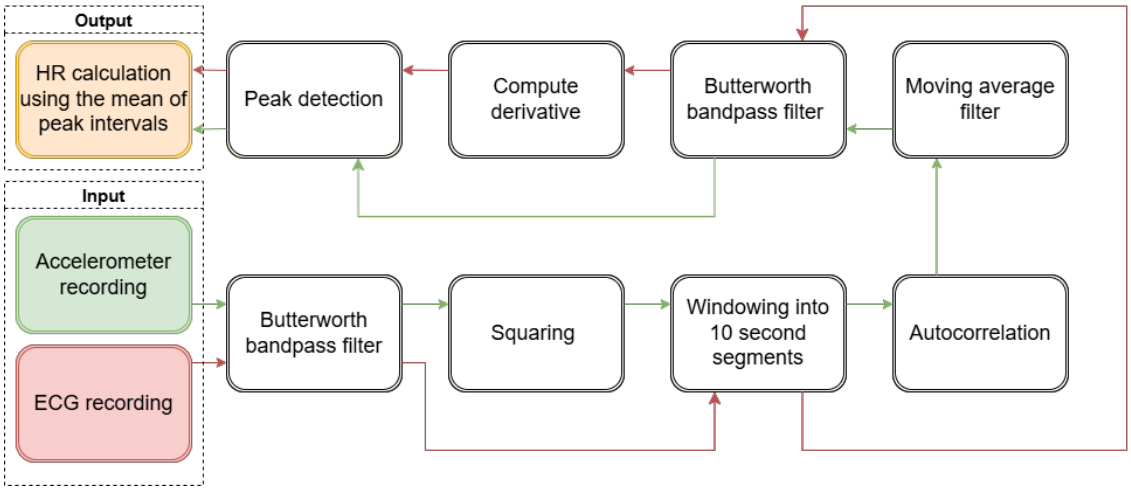

Figure 5.1: Proposed method pipeline

5.1 Pre-processing

The dataset contains 3-axis accelerometer data along with simultaneously recorded ECG-data. Both signals were captured with a sampling rate of 100 Hz, so resampling was not necessary. Similar to Haescher et al. [14], combining the three-dimensional accelerometer using the Euclidean formula was tested. However, as the ring was positioned upward during recording for each subject, it was concluded that the Y-axis contained the most relevant information overall. The algorithm was also tested on the X and Z axes individually, and in some cases, these axes produced the best estimations. The Y-axis however, still consistently provided the most reliable results overall and was therefore selected to be used for the analysis.

The accelerometer data was filtered using a bandpass filter with a passband of 0.5–15 Hz, while the ECG data was filtered with a passband of 0.5–12 Hz. These passbands were found to provide the best results, as they retained the heart rate components and filtered out most of the motion artifacts and other noise. Subsequently, the accelerometer data was processed using a squaring algorithm to emphasize the peaks produced by the heart cycles and to reduce the remaining noise. As in the ECG recordings, we were primarily interested in the R-peak locations, derivatives were computed for each signal to similarly enhance these peaks. Finally, the data was min-max normalized to the range of 0-1.

5.2 Autocorrelation process

At this point, the pre-processed data is ready for application of the autocorrelation function. The squaring algorithm has already highlighted the peaks corresponding to the heartbeats, and the autocorrelation function further emphasizes them, as seen in Figure 5.2. A 10-second window size was used for the autocorrelation, as this is the maximum delay permitted by standards from the American National Standards

Institute (ANSI) and the Association for the Advancement of Medical Instrumentation (AAMI) before a medical device must alert of unusual cardiorespiratory activity [56]. Selected window size also ensures the capture of multiple heart cycles. A 2-second step size was then used to slide the window forward, ensuring a sufficient number of data points for accurate analysis without compromising computational efficiency.

Since in the autocorrelation result, the second half is a mirror of the first, only the second half is used. The result is then further trimmed by removing 1.2 seconds from both the beginning and the end, to reduce the edge effects caused by the autocorrelation function. This step is highly important as edge effects can distort the signal, especially at the boundaries. Due to the 2 second windowing used in the analysis process, no data is lost when the edges are removed.

The trimmed autocorrelation function result is then smoothed using a moving average filter. A window size of 60 samples corresponding to 0.6 seconds is used, to ensure that the signal is properly smoothed, while also retaining the essential physiological features. The signal is subsequently processed with a bandpass filter (0.8-10 Hz to remove low-frequency baseline wander and high-frequency noise, making the peak detection process significantly less challenging. Finally, the signal is min-max normalized to a range of 0 to 1.

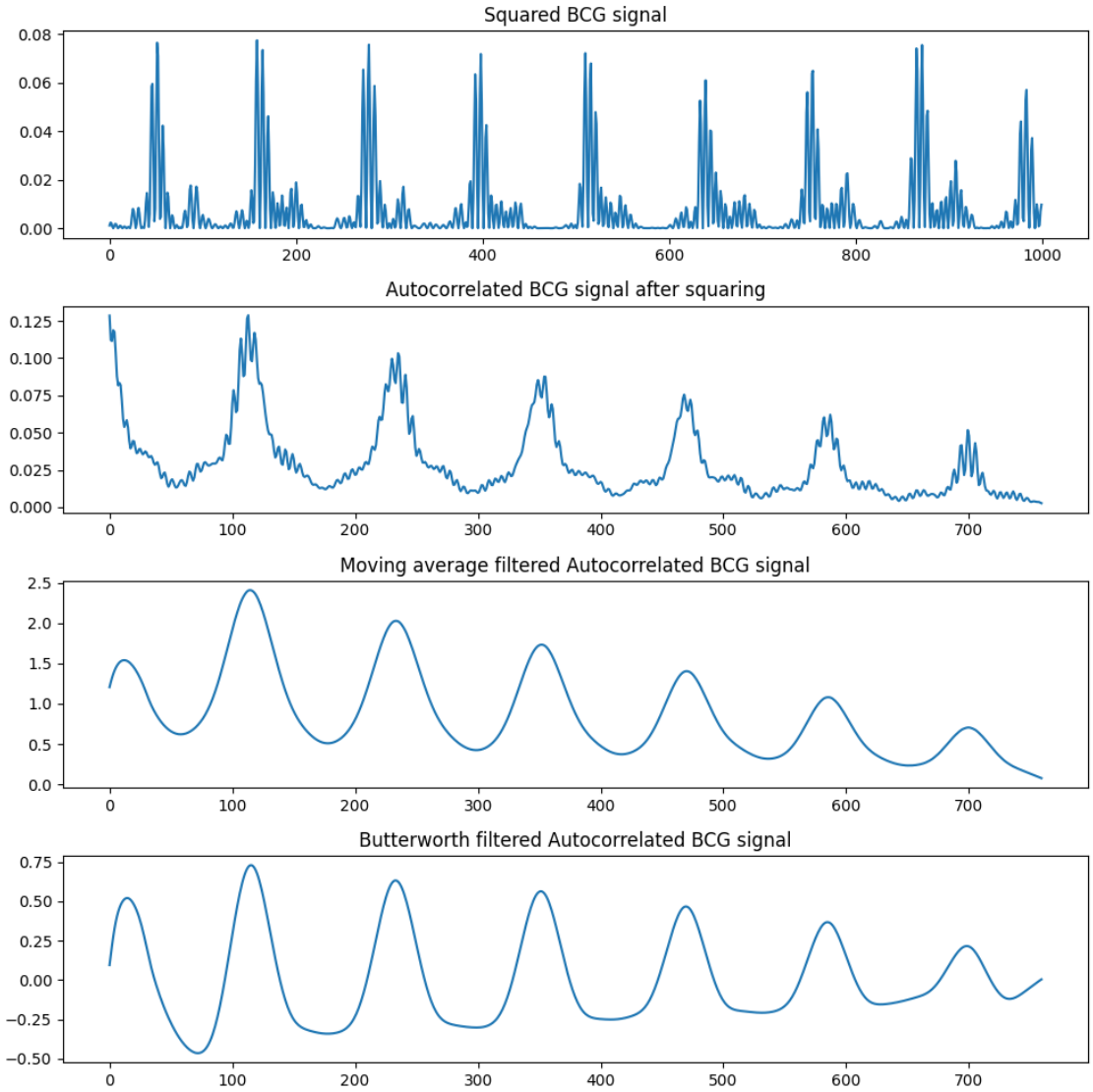

Figure 5.2: Autocorrelation process used in the algorithm. A squared 10-second BCG segment is autocorrelated and trimmed. The result is then smoothed and bandpass filtered.

5.3 Peak detection

To calculate the heart rates, a peak detection algorithm is applied to the signals. For the reference ECG, the widely used Pan-Tompkin's algorithm was employed for R-peak detection. This algorithm consists of a pre-processing stage, where the signal is prepared by removing remaining noise, smoothing, and increasing the QRS slope steepness, followed by a decision stage, where specific threshold values are used to determine the true peaks [70]. The concrete steps included in these two processes are quite similar to the algorithm used in this thesis for the accelerometer data processing. The ECG signal is first bandpass filtered, followed by extraction of the derivative and application of a squaring function to emphasize the R-peaks. The signal is then squared with a moving window integration, and finally in the decision stage the actual peaks are detected.

As the Pan-Tomkin's algorithm is designed for ECG signals, and the autocorrelation signal already undergoes a similar pre-processing stage, a different peak detection algorithm was employed for the BCG data. We use a modified automatic multiscale-based peak detection algorithm, which is specifically designed for biosignals with low signal-to-noise ratio, such as our BCG signal. The modified algorithm is based on Scholkmann's algorithm, where a local maxima scalogram matrix is constructed. By analyzing this matrix, the algorithm detects peaks and valleys by comparing the value of each data point to its neighbor at different scales [71].

For each 10 second BCG and ECG signal window, the peaks are calculated using these algorithms. The arrays containing the peaks are then used to calculate the heart rates by averaging the time differences between the peaks. By dividing 60 by this value, we obtain the heart rate in beats per minute (bpm).

5.4 Signal quality metrics

To estimate the possibility of implementing this type of heart rate calculation method in a wearable device several signal quality metrics were employed, to filter out BCG signals of poor quality. If the statistical metric values were not found to above certain threshold values, the segments were not used to calculate the heart rate.

Statistical measures skewness and kurtosis, that were introduced in Chapter 3.4, were used to detect signals that were clearly corrupted with different motion artifacts. These two metrics were calculated and used to assess the quality of the autocorrelation function.

In addition to these popular statistical metrics for signal quality assessment, a correlation coefficient was calculated to measure the similarity of a signal segment to itself. The correlation coefficient was computed by dividing the signal into two halves and calculating the coefficient for these segments. Since the measurements were taken from healthy subjects lying still, their heart rate can be assumed to remain relatively constant during the 10-second window, with no significant dysrhythmia expected. Any significant changes in the signal characteristics can be attributed to the motion artifacts present in the signal. However, a drawback of using the correlation coefficient as a signal quality metric is that physiological changes, such as arrhythmias can also affect the correlation coefficient. Autocorrelation has been successfully used to detect these irregularities from heart rate signals [72], [73] and if we want our algorithm to detect them, the use of the correlation coefficient might complicate this process.

Threshold values were selected for these signals through trial and error, as predefined values are difficult to set due to the influence of measurement devices and other study-specific parameters. When the threshold values were too high, some subjects' recordings were entirely discarded. and alternatively, when the threshold

values were set too low, their impact on the results was minimal, failing to filter noise effectively. However, suitable values were identified that helped reduce calculation errors compared to the ECG reference values.

6 Results

In this chapter, the results obtained from the smart ring device are presented. The accuracy of the estimated heart rates in comparison to the reference ECG values using several performance metrics. Additionally, Spearman's rank correlation analysis was conducted on each of the 23 subjects, to determine whether the heart rate estimations derived from the BCG signals correlate with the reference values. The effects of the signal quality metrics described in Section 5.4 are also reported.

6.1 Heart rate estimation

The purpose of this study was to study the possibility of estimating the heart rate with a wearable device using only the accelerometer data. Considering all 23 subjects, the results of the proposed algorithm were measured using several error metrics as a performance score. The results are displayed in Table 6.1. The used metrics are described below:

- The mean absolute error (MAE) [53], [74]:

$$MAE = \frac{1}{N}\sum_{i=1}^{N}|HR_{\text{Acc},i} - HR_{\text{ECG},i}|$$

- The median absolute error (MedAE) [74]:

$$MedAE = \text{median}(|HR_{\text{Acc},i} - HR_{\text{ECG},i}|)$$

- The root mean squared error (RMSE) [74], [75]:

$$RMSE = \sqrt{\frac{1}{N}\sum_{i=1}^{N}(HR_{\mathrm{Acc},i} - HR_{\mathrm{ECG},i})^2}$$

These metrics were chosen to get as wide a view as possible of the accuracy and the distribution of error in the HR estimations. With mean absolute error (MAE), we get a straightforward interpretation of how well the algorithm performed compared to the reference ECG.

From the mean absolute error values, we can observe that in most cases, the estimations fall well within the ±5 bpm range. However, from Figure 6.1 we can note, that in many signals there are large singular outliers. To reduce these singular outliers' effect on the error metric, the median absolute error (MedAE) is used, as it focuses on the middle of the error distribution and is less affected by the extreme values.

Finally, to also get a robust view of the outliers, the root mean squared error (RMSE) is used. As the errors are squared, the singular large values are more visible in the metric. For this reason, recordings with small MAE and a relatively large RMSE often indicate accurate estimations with a few extreme outliers.

Figure 6.1 compares the HR extracted from the BCG with reference ECG for each subject. From this we can observe considerable variance in the results. With some subjects, the BCG estimations follow the ECG reference relatively accurately. However, in some cases, such as Subject 21's estimations, there is a significant lack of correlation between the reference and the BCG. This is most likely due to poor signal quality, and in the case of Subject 21's signal, this was confirmed by visually examining the accelerometer data. In most signals, poor quality is likely due to motion artifacts. However, in the Subject 21's signal, in addition to a significant amount of noise, the sensor was poorly oriented upward, causing the x-axis to contain

more heart cycles than the y-axis.

In a broader view, most signals exhibit a clear correlation between the ECG HR and BCG HR estimation. In all signals except Subject 21, the MAE stays within the ± 5 bpm range. Additionally, in most cases, there are only a few significant outliers in the bpm estimations. The average MAE for heart rate estimations is 1.89 bpm (range: 0.29–11.69 bpm), the average MedAE is 1.08 bpm (range: 0.21–10.99 bpm), and the average RMSE is 3.45 bpm (range: 0.38–13.77 bpm).

Table 6.1: Error metrics without using the signal quality metrics.

Subject	**MAE**	**MedAE**	**RMSE**
Subject 1	3.0409	1.8957	4.202
Subject 2	0.4312	0.2331	0.9863
Subject 3	1.7121	0.6061	4.2723
Subject 4	1.6584	0.4769	5.1704
Subject 5	0.3274	0.2529	0.4435
Subject 6	0.9536	0.4485	1.9899
Subject 7	0.439	0.3323	0.6322
Subject 8	1.5689	0.6784	3.2512
Subject 9	2.343	1.0785	3.8427
Subject 10	2.2635	0.9889	4.9287
Subject 11	0.799	0.4664	1.5572
Subject 12	1.0216	0.2921	4.6652
Subject 13	1.0382	0.4295	2.4247
Subject 14	2.9107	0.7307	5.8215
Subject 15	1.1895	0.6615	2.2412
Subject 16	0.8783	0.4753	1.7066
Subject 17	3.5405	1.3227	7.1906
Subject 18	0.4572	0.2774	0.7326
Subject 19	0.2912	0.2093	0.3842
Subject 20	2.4585	1.1927	4.1661
Subject 21	11.6895	10.9888	13.7704
Subject 22	1.0837	0.4294	2.8146
Subject 23	1.1032	0.4441	2.2694
Average	1.8782	1.0831	3.4549

Table 6.2: Error metrics using the signal quality metrics.

Subject	**MAE**	**MedAE**	**RMSE**
Subject 1	2.3239	1.4392	3.3187
Subject 2	0.3953	0.2281	0.8968
Subject 3	0.8188	0.5835	1.0792
Subject 4	0.6568	0.3989	1.1752
Subject 5	0.2947	0.2485	0.3836
Subject 6	0.6433	0.4329	1.2294
Subject 7	0.3940	0.3223	0.5227
Subject 8	1.1012	0.6725	1.9727
Subject 9	1.8875	0.9989	3.2933
Subject 10	1.5089	0.7941	4.3716
Subject 11	0.5199	0.3736	0.6574
Subject 12	1.5401	0.3132	5.5187
Subject 13	0.5221	0.3382	1.2244
Subject 14	1.2504	0.5542	2.1700
Subject 15	0.6737	0.5199	0.9217
Subject 16	0.7670	0.4586	1.3131
Subject 17	3.7362	1.0696	8.1476
Subject 18	0.3734	0.2673	0.5199
Subject 19	0.2891	0.1974	0.3886
Subject 20	1.6354	1.2212	2.4596
Subject 21	9.4273	7.1292	10.4420
Subject 22	0.5533	0.3061	1.0505
Subject 23	0.8019	0.4013	1.8859
Average	1.3963	0.8378	2.3888

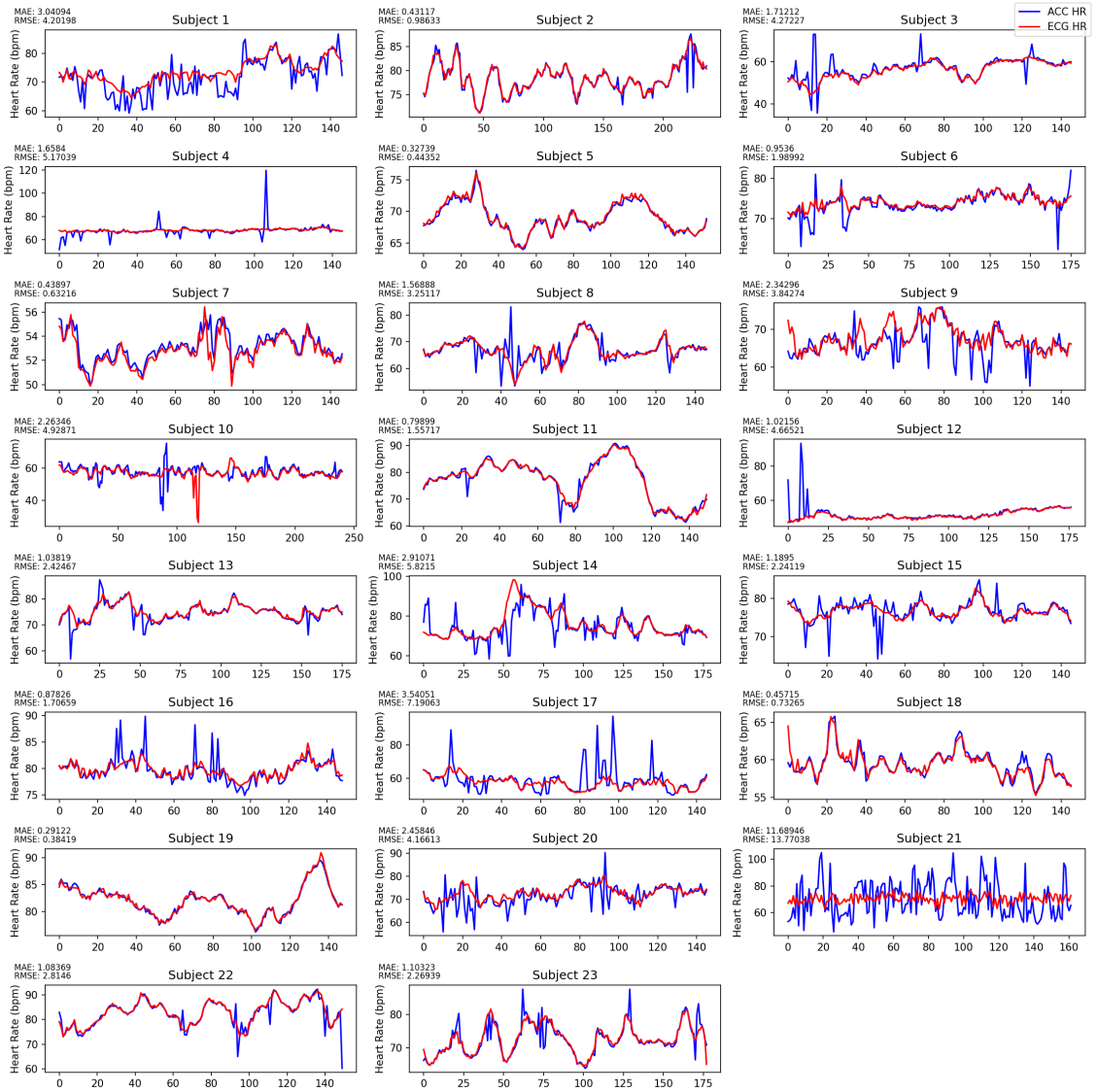

Figure 6.1: HR result comparison from each subject. Mean absolute error and root mean squared error relative to the ECG, is also shown in the graphs.

6.2 Signal quality metrics

The used signal quality metrics impact on the heart rate estimations by the proposed algorithm can be effectively observed, by comparing Table 6.1 and Table 6.2. The

most notable effect of these metrics, is the reduction of clear outliers, as indicated by the significantly lower average RMSE value (1.07 bpm). As mentioned in Section 6.1, the RMSE metric provides a broad view of extreme values. The clear decrease in this metric suggests that many of the extreme outlier values have been filtered out. This can also be detected by viewing Figure 6.1 and Figure 6.2, which show a noticeably lower amount of clear estimation spikes in the graphs.

The statistical metrics also have a noticeable effect on the MAE providing a better value in 21 out of 23 cases and a lower overall average of 0.48 bpm. The increased MAE in the two remaining subjects can be explained by the significantly reduced amount of estimations made for these signals. Initially the algorithm produces approximately 150 HR estimations per signal, but this drops to about 60 after the signal quality metric-based filtering. In both signals a few large outliers still remain as visible in Figure 6.2, and these outliers have a greater effect on the overall values produced by the metrics. This is further supported by the lower MedAE value in both cases after filtering, as MedAE is less sensitive to individual large outliers. Overall, the average MedAE decreases by 0.25 bpm, further reducing the already low median error.

The thresholds for the signal quality metrics were set in such a way, that each subject would have at least 1 eligible 10 second segment. Naturally, this means that if the signal quality is low, only a handful of segments may pass. From Figure 6.2, we can observe that, in the case of Subject 21, only a few windows passed the assessment. When the algorithm was ran without the signal quality estimation, 3738 windows were processed; when the signals with poor quality were filtered out, only 1599 remained, leaving us a coverage of 43% for the filtered results.

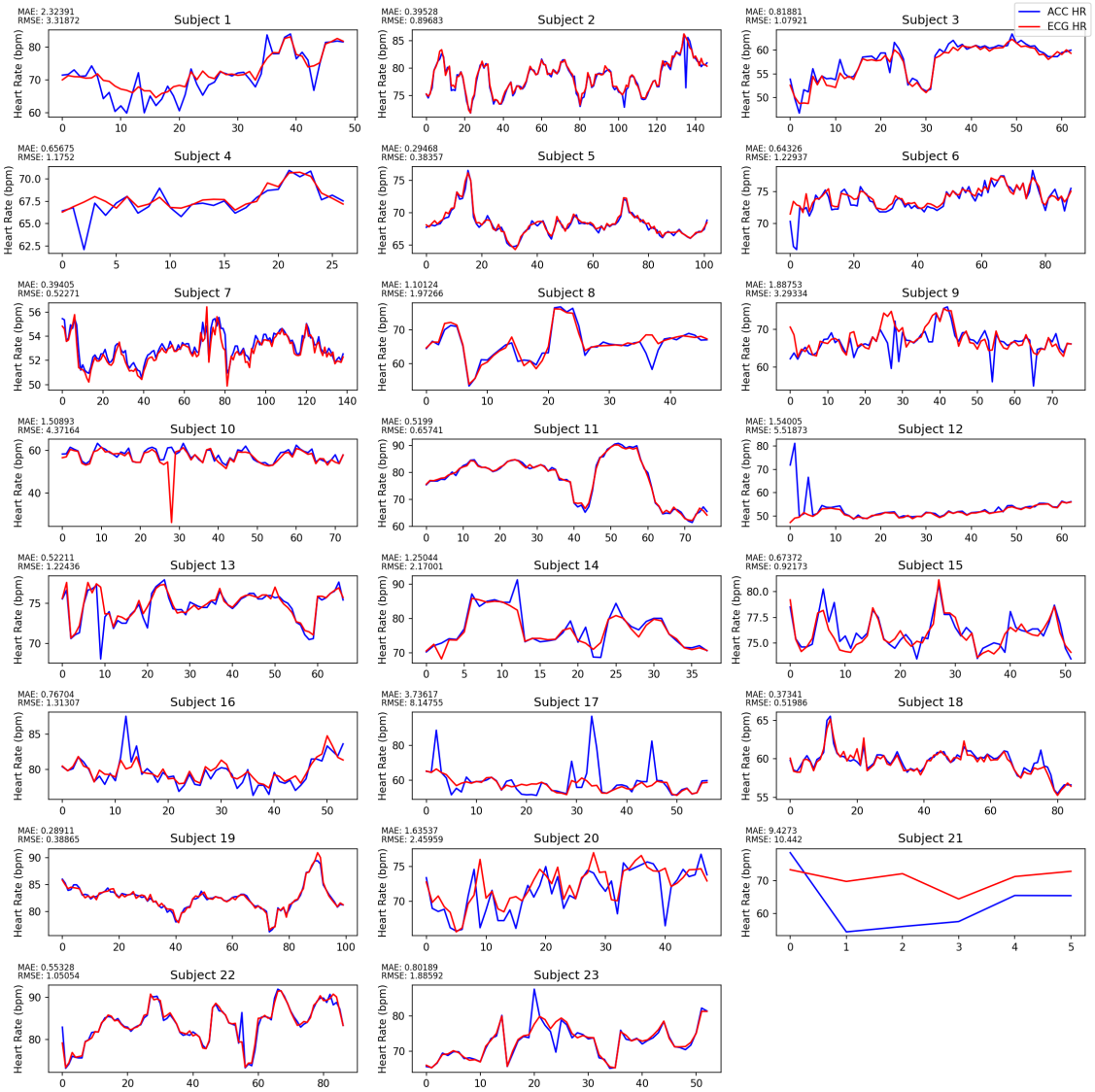

Figure 6.2: Comparison of heart rate results from each subject, excluding signals that did not meet the statistical threshold metrics. The effect of the filtration is clearly visible, as many subjects now have a significantly reduced number of analyzed signal windows, and in some cases, only a few signal segments are passed.

6.3 Correlation analysis

To evaluate the overall performance of the proposed algorithm more thoroughly, correlation analysis was performed. The correlation coefficients should provide a meaningful indicator of how well the proposed algorithms estimations correlate with the reference ECG heart rates.

Spearman's correlation coefficient describes the relationship between two variables, specifically capturing the strength and direction of this relationship [76]. The coefficient ranges from -1, indicating a perfect negative correlation, to 1, indicating a perfect positive correlation [76]. A positive correlation means that as one variable increases or decreases, the other does so similarly. Contrarily, a negative correlation implies that as one variable increases, the other decreases. As the value of this coefficient gets closer to 0, it suggests little to no linear correlation. In the case of this thesis, we of course aim for a high linear correlation between the proposed method ang ECG.

The Spearman's rank correlation test does not assume normality in the data and is robust to nonnormality [77]. The normality of the BCG and ECG arrays was tested with Shapiro-Wilk test [78], which concluded that, in most cases, the heart rate arrays are not normally distributed. Therefore, the correlation coefficient for each subject was calculated using the Spearman's rank correlation. The results without the statistical metrics are displayed in Table 6.3, while those with the metrics are shown in Table 6.4.

The null hypothesis of this statistical test is that there is no correlation between the two variables, and the significance level is usually set at 0.05 [79]. Both with and without the statistical metrics, we can observe that in all cases, except Subject 21, the p-value is clearly below this significance level, indicating that we can reject the null hypothesis. This suggests that the estimations for all other subjects show a clear positive correlation with the reference values. The error metric values from Table

Table 6.3: Correlation statistics without the signal quality metrics.

Subject	**Spearman Correlation Coefficient**	**p-value**
Subject 1	0.7701	4.22e-30
Subject 2	0.9531	5.51e-124
Subject 3	0.7884	3.41e-32
Subject 4	0.7571	2.06e-28
Subject 5	0.9779	6.82e-104
Subject 6	0.8777	1.74e-57
Subject 7	0.9213	2.30e-61
Subject 8	0.7297	1.03e-25
Subject 9	0.5435	1.36e-12
Subject 10	0.6222	3.19e-27
Subject 11	0.9827	3.24e-110
Subject 12	0.8791	3.27e-58
Subject 13	0.8931	2.90e-62
Subject 14	0.7335	2.48e-31
Subject 15	0.7801	4.02e-31
Subject 16	0.8916	1.91e-52
Subject 17	0.5310	5.37e-12
Subject 18	0.9000	8.49e-54
Subject 19	0.9869	1.56e-117
Subject 20	0.5978	1.62e-15
Subject 21	0.0898	0.26
Subject 22	0.9293	6.50e-66
Subject 23	0.9107	1.67e-69
Average	0.7846	0.0113

Table 6.4: Correlation statistics with the signal quality metrics.

Subject	**Spearman Correlation Coefficient**	**p-value**
Subject 1	0.849	1.22e-14
Subject 2	0.966	3.44e-87
Subject 3	0.958	8.66e-35
Subject 4	0.801	5.10e-07
Subject 5	0.959	9.85e-57
Subject 6	0.924	4.49e-38
Subject 7	0.947	1.91e-69
Subject 8	0.847	6.10e-14
Subject 9	0.612	4.76e-09
Subject 10	0.825	2.75e-19
Subject 11	0.990	3.57e-66
Subject 12	0.755	8.78e-13
Subject 13	0.883	4.87e-23
Subject 14	0.940	2.18e-18
Subject 15	0.812	2.65e-13
Subject 16	0.909	1.95e-21
Subject 17	0.624	2.19e-07
Subject 18	0.905	1.85e-32
Subject 19	0.967	9.88e-62
Subject 20	0.678	1.22e-07
Subject 21	0.600	0.28
Subject 22	0.962	1.00e-49
Subject 23	0.943	4.53e-26
Average	0.8546	0.0122

6.1 and Table 6.2 also support these results. The correlation coefficients indicate strong positive correlations, with an average of 0.79 (range: 0.0898–0.9869) without the statistical metrics, and 0.85 (range: 0.600–0.990) when the metrics are used.

To gain a better understanding of the overall correlation in the data, the estimates produced by the algorithm for all 23 subjects, along with their reference ECG values, are plotted in Figure 6.3. The plot clearly illustrates the pairwise relationships between the BCG and ECG estimations. The improvement in the overall Spearman correlation coefficient (approximately 0.056), visible in the plots, results from the clear reduction of outliers after filtration, as evident in the graphs. The estimations using the signal quality assessment-based filtration fit well with the fit-

ted linear line, indicating that the error between the estimations produced by the proposed method and the reference ECG values is small.

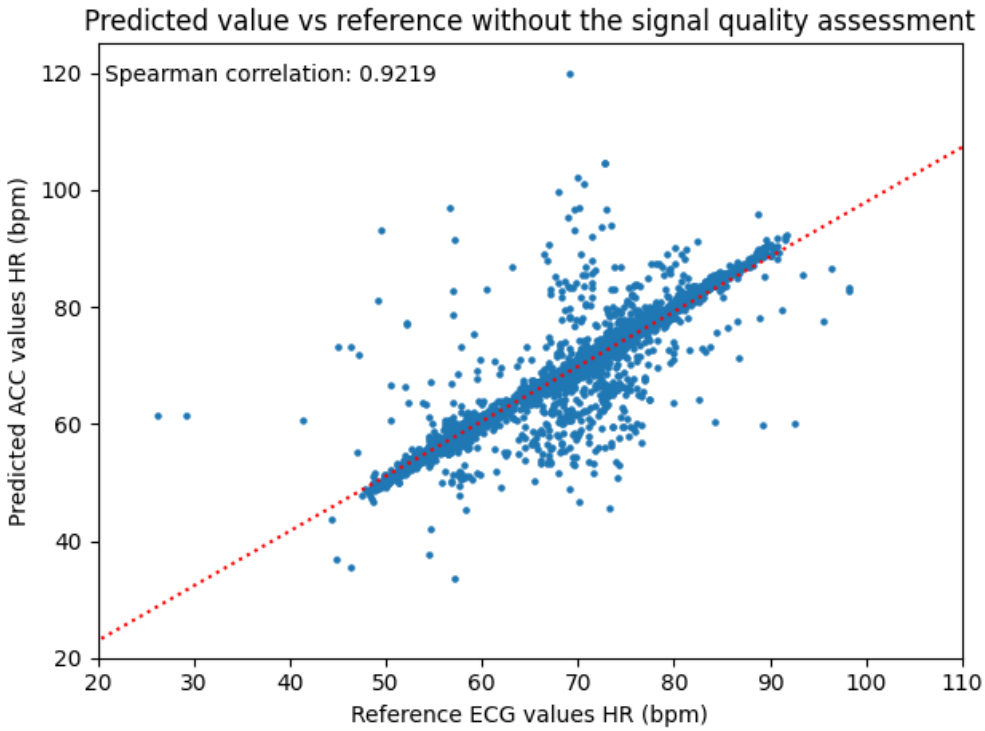

(a) Without signal quality assessment.

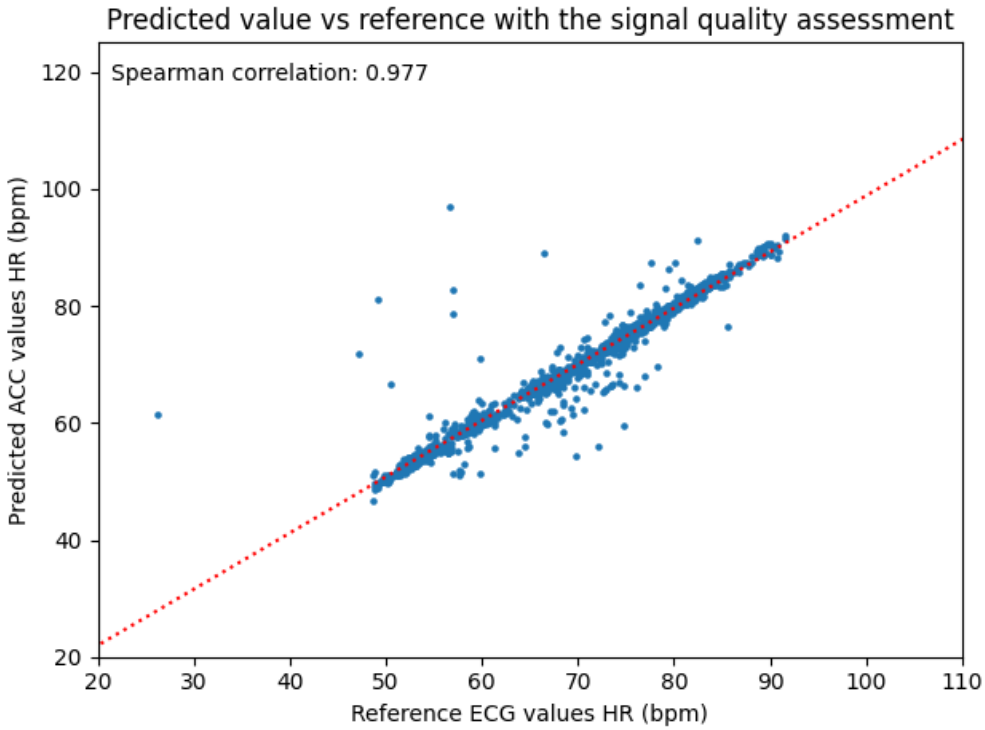

(b) With signal quality assessment.

Figure 6.3: The estimates produced by the proposed algorithm, alongside the reference ECG values, with and without the signal quality-based filtering. Spearman correlation coefficients are also included.

7 Discussion

When observing the results, we should focus on the MAE value as it effectively reflects how well the estimations fit within the ±5 bpm range, mentioned in Chapter 3.2. In our case, the MAE value is clearly below this range for all subjects except one. To further analyze how well the estimations fit within this range, a bar plot showing the error distributions between the BCG and reference ECG was created (7.1). Without the statistical signal quality assessment metrics, 3738 BCG windows were processed, and from these windows the estimations were within the ±5 bpm range 93.3% of the time. When using the statistical metrics, this percentage increased to 96.2%.

From Figure 7.1 we can observe that in both cases, the peak is close to 0 bpm, with most estimations falling within the range of ±2.5 bpm. Although these are resting heart rates, making it easier to meet the ±5 bpm range, this would suggest that the BCG data recorded from the finger contains enough relevant information to be potentially implemented in a wearable device.

This is further supported by the fact that the statistical measures used to assess the signal quality had clear positive impacts on the estimation results, as indicated by the error metrics and correlation tests. The fact that these relatively simple statistical metrics helped improve the already promising results obtained from the finger-worn accelerometer suggests that this technology could be introduced in a commercial device. The modern wearable devices already rely heavily on

accelerometers in sleep monitoring, so the implementation of this technology should not require any additional sensors on the devices. These statistical measures can also be replaced with more sophisticated motion artifact reduction and recognition techniques, such as using the accelerometer data itself as a reference signal for adaptive algorithms. Additionally, the potential of using the accelerometer data to select appropriate times for calculating heart rate, based on the subject's level of activity, should be studied.

A significant limitation of this study is the relatively small dataset used to assess the algorithm, with data recorded from only 23 subjects. Despite the dataset size, one signal was of clearly poor quality; Subject 21's recording was corrupted with noise and was improperly oriented. This also highlights another potential issue with the algorithm: when the ring is not oriented correctly, the estimations become inaccurate, as we only rely on the Y-axis. The possibility of adding the other axes, possibly with some coefficients, to still emphasize key axes or finding the best signal-specific axis should be studied further.

When visually examining the BCG signals, clear physiological impacts were noticeable; some subjects' recordings exhibited distinct peaks and easily identifiable heart cycles, while others had weaker signal amplitudes, even when free from motion artifacts.

The algorithm presented is a relatively simple approach to estimating heart rate from the BCG signal. The results are promising; however, this method is unlikely to perform well in scenarios involving subject movement or even when standing still. Although the algorithm should be tested further on noisy signals, it is unlikely to withstand significant motion artifacts.

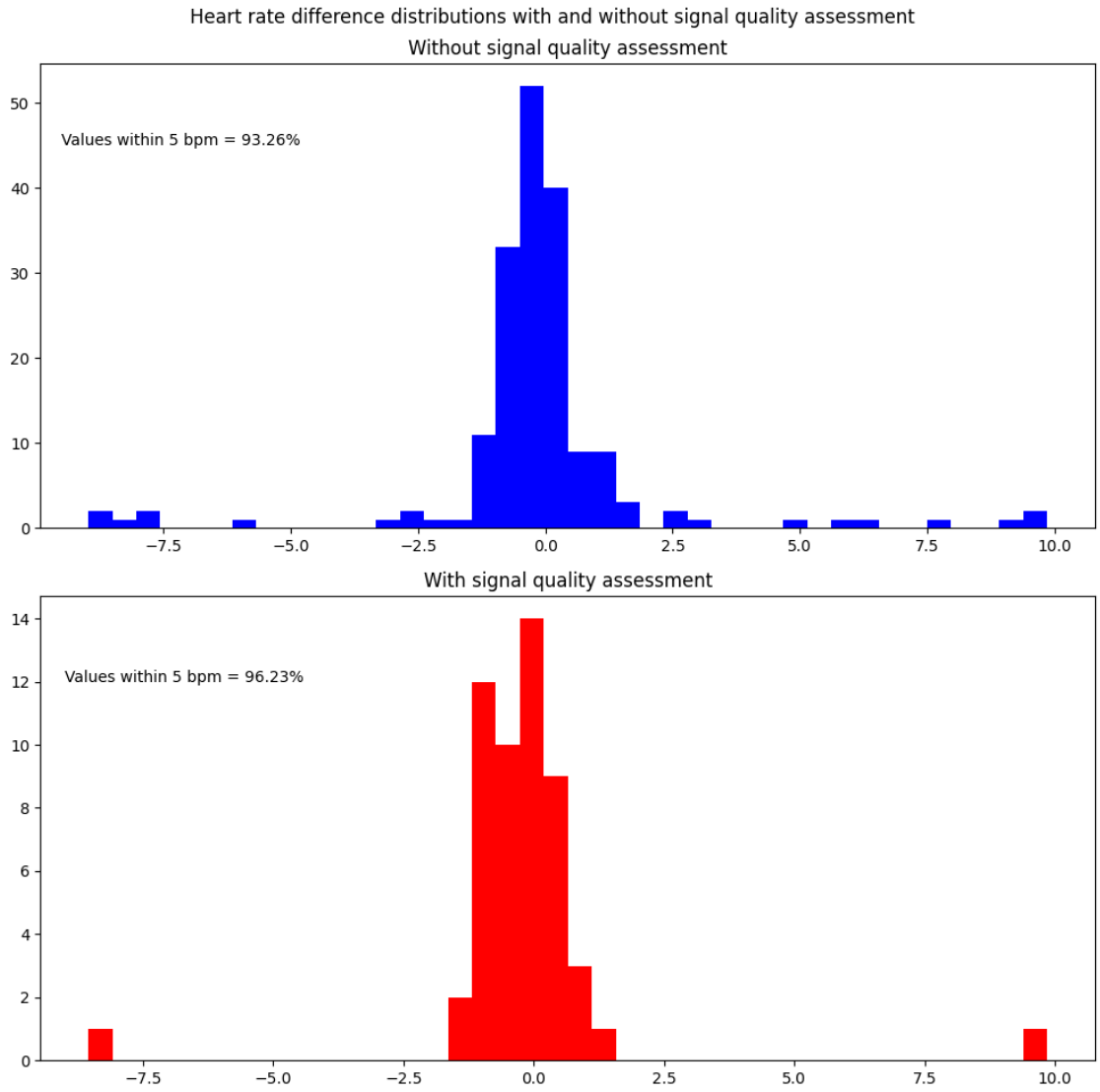

Figure 7.1: Bar plot describing the distribution of the estimation error compared to the reference ECG.

8 Conclusions

In this thesis, the goal was to study whether a finger-worn accelerometer sensor alone is capable of detecting heart rate with adequate accuracy. The primary motivation for this approach is the considerably lower power consumption of the accelerometer sensor compared to the industry standard PPG technology. Heart rate detection using an accelerometer sensor facilitates the optimization of battery life in wearable devices. Additionally, this study aimed to explore possibility of implementing the proposed method in a commercial smart ring for sleep and heart rate tracking.

As stated in Section 2.4, the advancements in accelerometer technology in recent years have significantly lowered the production costs of these sensors. Combined with the small size of the sensor unit and its low power consumption, this has enabled the widespread integration of accelerometers into modern wearable devices. This widespread availability is a clear advantage of the method proposed in this thesis, as it does not require additional sensors, making it already compatible with many existing wearable devices.

The results indicate that the accelerometer data alone can be used to approximate heart rate. By observing the Figure 7.1, we can see that even without the signal quality assessment the estimations were within the ± 5 bpm range 93% of the time. This is a very promising outcome, considering the relatively simple algorithm design. However, the proposed algorithm requires a fairly clean signal and is best suited for recordings taken in a resting position, as it is highly sensitive to noise.

When evaluating the possibility of implementing the algorithm proposed in this thesis in a commercial device, the impacts of using the signal quality-based filtration on the results was examined. The filtration had clear positive effects on the metrics used to evaluate the algorithm's accuracy and performance. The estimations were within the ± 5 bpm range 96% of the time (Figure 7.1), which is again, a highly promising result. This method is particularly well-suited for sleep tracking purposes, as the accelerometer signal contains minimal noise artifacts when the user is in a resting position during sleep, potentially allowing the smart rings to track sleep using only a single sensor.

References

[1] L. Lu, J. Zhang, Y. Xie, *et al.*, "Wearable health devices in health care: Narrative systematic review", *JMIR mHealth and uHealth*, vol. 8, no. 11, e18907, 2020.

[2] M. P. Turakhia, M. Desai, H. Hedlin, *et al.*, "Rationale and design of a large-scale, app-based study to identify cardiac arrhythmias using a smartwatch: The apple heart study", *American heart journal*, vol. 207, pp. 66–75, 2019.

[3] D. Insights, *Wearable technology in health care: Getting better all the time*, Accessed: 2024-11-25, 2021. [Online]. Available: `https://www2.deloitte.com/us/en/insights/industry/technology/technology-media-and-telecom-predictions/2022/wearable-technology-healthcare.html`.

[4] C. Downey, S. Chapman, R. Randell, J. Brown, and D. Jayne, "The impact of continuous versus intermittent vital signs monitoring in hospitals: A systematic review and narrative synthesis", *International journal of nursing studies*, vol. 84, pp. 19–27, 2018.

[5] S. Soon, H. Svavarsdottir, C. Downey, and D. G. Jayne, "Wearable devices for remote vital signs monitoring in the outpatient setting: An overview of the field", *BMJ Innovations*, vol. 6, no. 2, 2020.

[6] X. Chen, H. Zhang, Z. Li, S. Liu, Y. Zhou, *et al.*, "Continuous monitoring of heart rate variability and respiration for the remote diagnosis of chronic ob-

structive pulmonary disease: Prospective observational study", *JMIR mHealth and uHealth*, vol. 12, no. 1, e56226, 2024.

[7] A. A. Hernandez, P. Bonizzi, R. Peeters, and J. Karel, "Continuous monitoring of acute myocardial infarction with a 3-lead ecg system", *Biomedical Signal Processing and Control*, vol. 79, p. 104 041, 2023.

[8] M. A. Rosenberg, M. Samuel, A. Thosani, and P. J. Zimetbaum, "Use of a noninvasive continuous monitoring device in the management of atrial fibrillation: A pilot study", *Pacing and Clinical Electrophysiology*, vol. 36, no. 3, pp. 328–333, 2013.

[9] H. Zhou, T. Lu, Y. Liu, S. Zhang, R. Liu, and M. Gowda, "One ring to rule them all: An open source smartring platform for finger motion analytics and healthcare applications", in *Proceedings of the 8th ACM/IEEE Conference on Internet of Things Design and Implementation*, 2023, pp. 27–38.

[10] D. Lapsa, R. Janeliukstis, M. Metshein, and L. Selavo, "Ppg and bioimpedance-based wearable applications in heart rate monitoring—a comprehensive review", *Applied Sciences*, vol. 14, no. 17, p. 7451, 2024.

[11] M. A. Almarshad, M. S. Islam, S. Al-Ahmadi, and A. S. BaHammam, "Diagnostic features and potential applications of ppg signal in healthcare: A systematic review", in *Healthcare*, MDPI, vol. 10, 2022, p. 547.

[12] O. T. Inan, P.-F. Migeotte, K.-S. Park, *et al.*, "Ballistocardiography and seismocardiography: A review of recent advances", *IEEE journal of biomedical and health informatics*, vol. 19, no. 4, pp. 1414–1427, 2014.

[13] D. C. Deuchar, *Ballistocardiography: Introduction*, 1967.

[14] M. Haescher, D. J. Matthies, J. Trimpop, and B. Urban, "A study on measuring heart-and respiration-rate via wrist-worn accelerometer-based seismocardiography (scg) in comparison to commonly applied technologies", in *Proceed-*

ings of the 2nd international Workshop on Sensor-based Activity Recognition and Interaction, 2015, pp. 1–6.

[15] H. S. Kang and M. Exworthy, "Wearing the future—wearables to empower users to take greater responsibility for their health and care: Scoping review", *JMIR mHealth and uHealth*, vol. 10, no. 7, e35684, 2022.

[16] J. Dunn, R. Runge, and M. Snyder, "Wearables and the medical revolution", *Personalized medicine*, vol. 15, no. 5, pp. 429–448, 2018.

[17] U.S. Food and Drug Administration (FDA), *Summary of safety and effectiveness data (ssed): Dexcom g6 continuous glucose monitoring system*, DEN180044, 2018. [Online]. Available: `https://www.accessdata.fda.gov/cdrh_docs/pdf18/DEN180044.pdf`.

[18] U.S. Food and Drug Administration (FDA), *Fda clears first over-the-counter continuous glucose monitor*, Accessed: 2024-09-17, 2022. [Online]. Available: `https://www.fda.gov/news-events/press-announcements/fda-clears-first-over-counter-continuous-glucose-monitor`.

[19] Dexcom, Inc., *Dexcom stg*, Accessed: 2024-09-17, 2024. [Online]. Available: `https://provider.dexcom.com/stelo`.

[20] L. Lyzwinski, M. Elgendi, and C. Menon, "Innovative approaches to menstruation and fertility tracking using wearable reproductive health technology: Systematic review", *Journal of Medical Internet Research*, vol. 26, e45139, 2024.

[21] M. Yenikomshian, J. Jarvis, C. Patton, *et al.*, "Cardiac arrhythmia detection outcomes among patients monitored with the zio patch system: A systematic literature review", *Current Medical Research and Opinion*, vol. 35, no. 10, pp. 1659–1670, 2019.

[22] D. Castaneda, A. Esparza, M. Ghamari, C. Soltanpur, and H. Nazeran, "A review on wearable photoplethysmography sensors and their potential future applications in health care", *International journal of biosensors & bioelectronics*, vol. 4, no. 4, p. 195, 2018.

[23] J. Lee, K. Matsumura, K.-i. Yamakoshi, P. Rolfe, S. Tanaka, and T. Yamakoshi, "Comparison between red, green and blue light reflection photoplethysmography for heart rate monitoring during motion", in *2013 35th annual international conference of the IEEE engineering in medicine and biology society (EMBC)*, IEEE, 2013, pp. 1724–1727.

[24] A. Moço and W. Verkruysse, "Pulse oximetry based on photoplethysmography imaging with red and green light: Calibratability and challenges", *Journal of clinical monitoring and computing*, vol. 35, no. 1, pp. 123–133, 2021.

[25] J. L. Moraes, M. X. Rocha, G. G. Vasconcelos, J. E. Vasconcelos Filho, V. H. C. De Albuquerque, and A. R. Alexandria, "Advances in photopletysmography signal analysis for biomedical applications", *Sensors*, vol. 18, no. 6, p. 1894, 2018.

[26] A. Abushouk, T. Kansara, O. Abdelfattah, *et al.*, "The dicrotic notch: Mechanisms, characteristics, and clinical correlations", *Current Cardiology Reports*, vol. 25, no. 8, pp. 807–816, 2023.

[27] A. L. Goldberger, Z. D. Goldberger, and A. Shvilkin, "Chapter 1 - essential concepts: What is an ecg?", in *Goldberger's Clinical Electrocardiography (Ninth Edition)*, A. L. Goldberger, Z. D. Goldberger, and A. Shvilkin, Eds., Ninth Edition, Elsevier, 2018, pp. 2–5, ISBN: 978-0-323-40169-2. DOI: https://doi.org/10.1016/B978-0-323-40169-2.00001-9. [Online]. Available: https://www.sciencedirect.com/science/article/pii/B9780323401692000019.

[28] Y. Sattar and L. Chhabra, "Electrocardiogram", in *StatPearls [Internet]*, StatPearls Publishing, 2023.

[29] A. L. Goldberger, Z. D. Goldberger, and A. Shvilkin, "Chapter 2 - ecg basics: Waves, intervals, and segments", in *Goldberger's Clinical Electrocardiography (Ninth Edition)*, A. L. Goldberger, Z. D. Goldberger, and A. Shvilkin, Eds., Ninth Edition, Elsevier, 2018, pp. 6–10, ISBN: 978-0-323-40169-2. DOI: https://doi.org/10.1016/B978-0-323-40169-2.00002-0. [Online]. Available: https://www.sciencedirect.com/science/article/pii/B9780323401692000020.

[30] A. H. Kashou, H. Basit, and L. Chhabra, "Physiology, sinoatrial node", 2017.

[31] Z. F. Issa, J. M. Miller, and D. P. Zipes, "10 - intraventricular conduction abnormalities", in *Clinical Arrhythmology and Electrophysiology (Third Edition)*, Z. F. Issa, J. M. Miller, and D. P. Zipes, Eds., Third Edition, Philadelphia: Elsevier, 2019, pp. 286–304, ISBN: 978-0-323-52356-1. DOI: https://doi.org/10.1016/B978-0-323-52356-1.00010-4. [Online]. Available: https://www.sciencedirect.com/science/article/pii/B9780323523561000104.

[32] A. L. Goldberger, Z. D. Goldberger, and A. Shvilkin, "Chapter 4 - ecg leads", in *Goldberger's Clinical Electrocardiography (Ninth Edition)*, A. L. Goldberger, Z. D. Goldberger, and A. Shvilkin, Eds., Ninth Edition, Elsevier, 2018, pp. 21–31, ISBN: 978-0-323-40169-2. DOI: https://doi.org/10.1016/B978-0-323-40169-2.00004-4. [Online]. Available: https://www.sciencedirect.com/science/article/pii/B9780323401692000044.

[33] T. M. Pereira, R. C. Conceição, V. Sencadas, and R. Sebastião, "Biometric recognition: A systematic review on electrocardiogram data acquisition methods", *Sensors*, vol. 23, no. 3, p. 1507, 2023.

[34] D. Arvidsson, J. Fridolfsson, and M. Börjesson, "Measurement of physical activity in clinical practice using accelerometers", *Journal of internal medicine*, vol. 286, no. 2, pp. 137–153, 2019.

[35] C.-C. Yang and Y.-L. Hsu, "A review of accelerometry-based wearable motion detectors for physical activity monitoring", *Sensors*, vol. 10, no. 8, pp. 7772–7788, 2010.

[36] L. Giovangrandi, O. T. Inan, R. M. Wiard, M. Etemadi, and G. T. Kovacs, "Ballistocardiography—a method worth revisiting", in *2011 annual international conference of the IEEE engineering in medicine and biology society*, IEEE, 2011, pp. 4279–4282.

[37] J. Alametsä, J. Viik, J. Alakare, A. Värri, and A. Palomäki, "Ballistocardiography in sitting and horizontal positions", *Physiological measurement*, vol. 29, no. 9, p. 1071, 2008.

[38] I. Elnaggar, T. Hurnanen, J. Sandelin, *et al.*, "Multichannel bed based ballistocardiography heart rate estimation using continuous wavelet transforms and autocorrelation", in *2022 Computing in Cardiology (CinC)*, IEEE, vol. 498, 2022, pp. 1–4.

[39] R. Gargees, J. M. Keller, M. Popescu, and M. Skubic, "Non-invasive classification of sleep stages with a hydraulic bed sensor using deep learning", in *How AI Impacts Urban Living and Public Health: 17th International Conference, ICOST 2019, New York City, NY, USA, October 14-16, 2019, Proceedings 17*, Springer, 2019, pp. 73–82.

[40] O. T. Inan, "Recent advances in cardiovascular monitoring using ballistocardiography", in *2012 Annual international conference of the IEEE engineering in medicine and biology society*, IEEE, 2012, pp. 5038–5041.

[41] J. Feng, W. Huang, J. Jiang, *et al.*, "Non-invasive monitoring of cardiac function through ballistocardiogram: An algorithm integrating short-time fourier transform and ensemble empirical mode decomposition", *Frontiers in Physiology*, vol. 14, p. 1 201 722, 2023.

[42] E. Vogt, D. MacQuarrie, and J. P. Neary, "Using ballistocardiography to measure cardiac performance: A brief review of its history and future significance", *Clinical physiology and functional imaging*, vol. 32, no. 6, pp. 415–420, 2012.

[43] S. W. Smith, "The scientist and engineer's guide to digital signal processing", *California Technical Pub*, pp. 261–262, 1997.

[44] S. F. Hussin, G. Birasamy, and Z. Hamid, "Design of butterworth band-pass filter", *Politeknik & Kolej Komuniti Journal of Engineering and Technology*, vol. 1, no. 1, pp. 32–46, 2016.

[45] M. Shouran and E. Elgamli, "Design and implementation of butterworth filter", *International Journal of Innovative Research in Science Engineering and Technology*, vol. 9, no. 9, pp. 7975–7983, 2020.

[46] J. L. Guiñón, E. Ortega, J. García-Antón, and V. Pérez-Herranz, "Moving average and savitzki-golay smoothing filters using mathcad", *Papers ICEE*, vol. 2007, pp. 1–4, 2007.

[47] E. Guillodo, C. Lemey, M. Simonnet, *et al.*, "Clinical applications of mobile health wearable–based sleep monitoring: Systematic review", *JMIR mHealth and uHealth*, vol. 8, no. 4, e10733, 2020.

[48] A. K. Patel, V. Reddy, K. R. Shumway, and J. F. Araujo, "Physiology, sleep stages", in *StatPearls [Internet]*, StatPearls Publishing, 2024.

[49] J. L. Aldredge and A. J. Welch, "Variations of heart rate during sleep as a function of the sleep cycle", *Electroencephalography and Clinical Neurophysiology*, vol. 35, no. 2, pp. 193–198, 1973.

[50] P. Yousefian, S. Shin, A. S. Mousavi, *et al.*, "Pulse transit time-pulse wave analysis fusion based on wearable wrist ballistocardiogram for cuff-less blood pressure trend tracking", *IEEE Access*, vol. 8, pp. 138 077–138 087, 2020.

[51] M. Moebus, L. Hauptmann, N. Kopp, B. U. Demirel, B. Braun, and C. Holz, "Nightbeat: Heart rate estimation from a wrist-worn accelerometer during sleep", in *IEEE-EMBS International Conference on Biomedical and Health Informatics*.

[52] H. Abdi and L. J. Williams, "Tukey's honestly significant difference (hsd) test", *Encyclopedia of research design*, vol. 3, no. 1, pp. 1–5, 2010.

[53] C. Zhao, W. Zeng, D. Hu, and H. Liu, "Robust heart rate monitoring by a single wrist-worn accelerometer based on signal decomposition", *IEEE Sensors Journal*, vol. 21, no. 14, pp. 15 962–15 971, 2021.

[54] H. Hassani, M. Royer-Carenzi, L. M. Mashhad, M. Yarmohammadi, and M. R. Yeganegi, "Exploring the depths of the autocorrelation function: Its departure from normality", *Information*, vol. 15, no. 8, p. 449, 2024.

[55] M. Laurino, D. Menicucci, A. Gemignani, N. Carbonaro, and A. Tognetti, "Moving auto-correlation window approach for heart rate estimation in ballistocardiography extracted by mattress-integrated accelerometers", *Sensors*, vol. 20, no. 18, p. 5438, 2020.

[56] Y. D'Mello, J. Skoric, S. Xu, *et al.*, "Autocorrelated differential algorithm for real-time seismocardiography analysis", *IEEE Sensors Journal*, vol. 19, no. 13, pp. 5127–5140, 2019.

[57] H. Lee, E. Kim, Y. Lee, *et al.*, "Toward all-day wearable health monitoring: An ultralow-power, reflective organic pulse oximetry sensing patch", *Science advances*, vol. 4, no. 11, eaas9530, 2018.

[58] P. K. Baheti and H. Garudadri, "An ultra low power pulse oximeter sensor based on compressed sensing", in *2009 sixth international workshop on wearable and implantable body sensor networks*, IEEE, 2009, pp. 144–148.

[59] Q. Liu, J. Williamson, K. Li, *et al.*, "Gazelle: Energy-efficient wearable analysis for running", *IEEE Transactions on Mobile Computing*, vol. 16, no. 9, pp. 2531–2544, 2016.

[60] N. Twomey, T. Diethe, X. Fafoutis, *et al.*, "A comprehensive study of activity recognition using accelerometers", in *Informatics*, MDPI, vol. 5, 2018, p. 27.

[61] H. Weinberg, "Minimizing power consumption of imems accelerometers", *Analog Devices*, 2002.

[62] S. Béres, L. Holczer, and L. Hejjel, "On the minimal adequate sampling frequency of the photoplethysmogram for pulse rate monitoring and heart rate variability analysis in mobile and wearable technology", *Measurement Science Review*, vol. 19, no. 5, pp. 232–240, 2019.

[63] Y. Liu, Y. Xiao, and Q. Fu, "A low power consumption inverter-based interface for capacitive accelerometer", *IEICE Electronics Express*, vol. 15, no. 1, pp. 20 171 152–20 171 152, 2018.

[64] B. V. Amini, R. Abdolvand, and F. Ayazi, "A 4.5-mw closed-loop micro-gravity cmos soi accelerometer", *IEEE Journal of Solid-State Circuits*, vol. 41, no. 12, pp. 2983–2991, 2006.

[65] D. P. Sergio and R. Diniz, *Adaptive filtering: Algorithms and practical implementation*, 2002.

[66] D. Pollreisz and N. TaheriNejad, "Detection and removal of motion artifacts in ppg signals", *Mobile Networks and Applications*, vol. 27, no. 2, pp. 728–738, 2022.

[67] M.-Z. Poh, N. C. Swenson, and R. W. Picard, "Motion-tolerant magnetic earring sensor and wireless earpiece for wearable photoplethysmography", *IEEE Transactions on Information Technology in Biomedicine*, vol. 14, no. 3, pp. 786–794, 2010.

[68] S. Nabavi and S. Bhadra, "A robust fusion method for motion artifacts reduction in photoplethysmography signal", *IEEE Transactions on Instrumentation and Measurement*, vol. 69, no. 12, pp. 9599–9608, 2020.

[69] R. Krishnan, B. Natarajan, and S. Warren, "Two-stage approach for detection and reduction of motion artifacts in photoplethysmographic data", *IEEE transactions on biomedical engineering*, vol. 57, no. 8, pp. 1867–1876, 2010.

[70] M. Fariha, R. Ikeura, S. Hayakawa, and S. Tsutsumi, "Analysis of pan-tompkins algorithm performance with noisy ecg signals", in *Journal of Physics: Conference Series*, IOP Publishing, vol. 1532, 2020, p. 012 022.

[71] S. M. Bishop and A. Ercole, "Multi-scale peak and trough detection optimised for periodic and quasi-periodic neuroscience data", in *Intracranial Pressure & Neuromonitoring XVI*, Springer, 2018, pp. 189–195.

[72] M. S. B. Sinal and E. Kamioka, "An efficient arrhythmia detection using autocorrelation and statistical approach", *Journal of Computer and Communications*, vol. 6, no. 10, pp. 63–81, 2018.

[73] E.-S. Väliaho, P. Kuoppa, J. A. Lipponen, *et al.*, "Wrist band photoplethysmography autocorrelation analysis enables detection of atrial fibrillation without pulse detection", *Frontiers in Physiology*, vol. 12, p. 654 555, 2021.

[74] A. Botchkarev, "Performance metrics (error measures) in machine learning regression, forecasting and prognostics: Properties and typology", *arXiv preprint arXiv:1809.03006*, 2018.

[75] M. Oyeleye, T. Chen, S. Titarenko, and G. Antoniou, "A predictive analysis of heart rates using machine learning techniques", *International Journal of Environmental Research and Public Health*, vol. 19, no. 4, p. 2417, 2022.

[76] K. Ali Abd Al-Hameed, "Spearman's correlation coefficient in statistical analysis", *International Journal of Nonlinear Analysis and Applications*, vol. 13, no. 1, pp. 3249–3255, 2022.

[77] A. J. Bishara and J. B. Hittner, "Confidence intervals for correlations when data are not normal", *Behavior research methods*, vol. 49, pp. 294–309, 2017.

[78] S. G. Kwak and S.-H. Park, "Normality test in clinical research", *Journal of Rheumatic Diseases*, vol. 26, no. 1, pp. 5–11, 2019.

[79] "Spearman rank correlation coefficient", in *The Concise Encyclopedia of Statistics*. New York, NY: Springer New York, 2008, pp. 502–505, ISBN: 978-0-387-32833-1. DOI: 10.1007/978-0-387-32833-1_379. [Online]. Available: https://doi.org/10.1007/978-0-387-32833-1_379.